

1   **Anthropogenic activity and climate change exacerbate the spread of**  
2   **pathogenic bacteria in the environment**

3   Yu Geng<sup>1</sup>, Ya Liu<sup>2,3,\*</sup>, Peng Li<sup>1</sup>, Jingyu Sun<sup>1</sup>, Yiru Jiang<sup>1</sup>, Zhuo Pan<sup>1</sup>, Yue-zhong Li<sup>1</sup>,  
4   Zheng Zhang<sup>1,\*</sup>

5   <sup>1</sup> State Key Laboratory of Microbial Technology, Institute of Microbial Technology,  
6   Shandong University, Qingdao 266237, China

7   <sup>2</sup> Qilu Hospital (Qingdao), Cheeloo College of Medicine, Shandong University,  
8   Qingdao 266035, China

9   <sup>3</sup> Suzhou Research Institute, Shandong University, Suzhou 215123, China

10   \* Corresponding author. Email: liuya@sdu.edu.cn (Y.L.), zhangzheng@sdu.edu.cn  
11   (Z.Z.); ORCID: 0000-0002-1756-0907 (Y.L.), 0000-0001-9971-6006 (Z.Z.)

12   **Short Title:** Climate change increases pathogenic bacteria risk

13   **Abstract**

14   Climate change is profoundly impacting human health. Human pathogenic bacteria  
15   (HPB) infections mediated by the environment are considered a substantial cause of  
16   global health losses. However, the biogeography of HPB and their response to climate  
17   change remain largely unknown. Here, we constructed and analyzed a global atlas of  
18   potential HPB using 1,066,584 samples worldwide. HPB are widely present in the  
19   global environment, and their distribution follows a latitudinal diversity gradient.  
20   Climate and anthropogenic factors are identified as major drivers of the global  
21   distribution of HPB. Our predictions indicated that by the end of this century, the  
22   richness, abundance, and invasion risk of HPB will increase globally, with this upward  
23   trend becoming more pronounced as development sustainability declines. Therefore,  
24   the threat of environmentally mediated HPB infections to human health may be more  
25   severe in a world where anthropogenic activities are intensifying and the global climate  
26   is warming.

27   **Teaser:** Climate change and human activity will increase global richness and  
28   abundance of pathogenic bacteria, threatening public health.

29 **Introduction**

30 Climate change may be the greatest health threat of the twenty-first century, impacting  
31 lives both directly and indirectly through the disruption of environmental and social  
32 determinants of health (1-4). Meta-analyses have indicated that human infectious  
33 diseases caused by pathogenic microorganisms are exacerbated by climate change (5-  
34 7). One of the most critical issues we need to consider is how climate change alters and  
35 intensifies the spread of pathogenic bacteria, parasites, fungi, and viruses (8).

36 Changes in climate and land use will cause species to aggregate in new combinations,  
37 facilitating cross-species transmission of viruses (9). Increased heat tolerance in fungi  
38 with pathogenic potential due to global warming could lead to new fungal diseases (10).  
39 Compared with nonbacterial etiologies, such as fungal infections, malaria, and HIV,  
40 infections caused by human pathogenic bacteria (HPB) are the second leading cause of  
41 death globally. Annually, bacterial infections contribute to an estimated 7.7 million  
42 deaths worldwide (11, 12). Specifically, environmentally mediated transmission is  
43 common among human pathogens, and contact with pathogens through water, food,  
44 waste, animals, or insect vectors contributes to a major burden of human disease (13).  
45 The concept of "One Health" emphasizes that the health of humans, domestic and wild  
46 animals, plants, and the wider environment (including ecosystems) are closely linked  
47 (14). Despite recent individual studies highlighting pathogen contamination and health  
48 risks in environments such as soil (15, 16), wastewater (17), groundwater (18), and  
49 ocean (19), there remains a lack of systematic analysis on the distribution characteristics  
50 and drivers of HPB in global ecosystems, and the potential impact of climate change  
51 on HPB has not been quantified.

52 Environmental DNA technology allows for the direct extraction of DNA from the  
53 environment without relying on pathogen isolation and microscopy, substantially  
54 facilitating research on environmental HPB (20, 21). The genetic information of  
55 bacteria obtained by 16S ribosomal RNA (rRNA) amplicon sequencing could be  
56 compared with human pathogen databases to reveal the composition, abundance, and  
57 distribution of potential HPB in the environment (22). The rapid accumulation of global  
58 catalogues of HPB and the extensive sequencing of microbial communities have made  
59 it possible to interpret the global distribution and potential health risks of HPB through  
60 big data analysis (23). Here, we conducted detection for HPB in more than one million  
61 microbial communities across global ecosystems. Through a series of theoretical and  
62 modeling methods, we (i) determined the taxonomic composition and distribution of  
63 potential HPB in the environment, (ii) mapped their global distribution and revealed the  
64 drivers of the richness and abundance of HPB, and (iii) predicted changes in HPB  
65 richness and invasion risk under future climate change scenarios.

66

67 **Results**

68 **The natural environment has emerged as a reservoir for HPB**

We conducted detection for HPB in 1,066,584 sequenced microbial communities, sourced from habitats including animal, plant, soil, and aquatic globally, excluding human-associated habitats (**fig. S1**). HPB were identified in up to 88% of these natural communities. The detected HPB belonged to 9 phyla, 16 classes, 36 orders, 69 families, 113 genera, and 330 species (**table S1**). Nearly 90% of these species were predominantly found in the phyla Pseudomonadota, Bacillota, Actinomycetota, and Bacteroidota (**Fig. 1A**). HPB in natural communities exhibited a latitudinal diversity gradient (LDG), with both their richness (Pearson's  $r = -0.15$   $P < 0.0001$ ) and relative abundance (Pearson's  $r = -0.14$ ,  $P < 0.0001$ ) showing weak yet significant negative correlations with absolute latitude (**Fig. 1, B and C**). On a continental scale, the detection rate (96%), richness (determined based on the operational taxonomic unit number of HPB in the microbial communities, median: 9), and relative abundance (parts per million, ppm, median: 3046.0) of HPB in natural communities were highest in Africa, followed by Asia (detection rate: 92%; richness: 9; relative abundance: 1273.0), whereas Antarctica exhibited the lowest values (detection rate: 69%; richness: 2; relative abundance: 53.7) (**Fig. 1, D to F**).

In terms of various habitats, the detection rates, richness, and relative abundance of HPB were significantly greater in animal-associated (excluding human-associated) habitats than in plant-associated, soil, and aquatic habitats (**Fig. 1, D to F and fig. S2**). Specifically, the detection rates of HPB in six animal-associated habitats were not less than 93%, with higher richness and relative abundance observed in pet and primate habitats, and lower values in fish and insecta habitats. Among the four plant-associated habitats, seed exhibited the highest detection rate, richness, and relative abundance of HPB, whereas wood demonstrated the lowest values. Across the eight soil habitats, these three metrics ranked the highest in farm and the lowest in tundra. In eight aquatic habitats, the three values of waste water were the highest, and those of marine were the lowest. In particular, the detection rates, richness, and relative abundance of HPB in anthropogenic habitats, such as pet, livestock, primate, farm, agricultural, and waste water, were significantly higher than those in natural habitats (**fig. S2**).

Based on the potential pathogenicity of HPB, detection rates across different continents ranged from 28% (Antarctica, Skin/Soft tissue) to 91% (Africa, Digestive system), while detection rates in various habitats varied between 23% (tundra, Skin/Soft tissue) and 97% (bird, Digestive system) (**Fig. 1G**). The richness of HPB, which targets the digestive system, was highest in almost all habitat types, whereas the lowest richness was observed for HPB which targets skin/soft tissue. From the perspective of HPB biosafety, the detection rates for BSL-1 ranged from 16% (tundra) to 88% (primate), those for BSL-2 varied between 46% (tundra) and 98% (primate), and those for BSL-3 ranged from 17% (primate) to 52% (farm) (**Fig. 1H**). In brief, HPB are widely present in domestic and wild animals, plants, as well as broader soil and aquatic environments, supporting the concept of "One Health", which closely links human health with the natural environment.

## **Anthropogenic activities facilitate the transmission of HPB among environments**

Pathogenic bacteria are closely associated with humans, and we evaluated the

relationships between anthropogenic activities and HPB in the environment using collected indicators (**table S2**). The richness of HPB in natural communities was significantly negatively correlated with life expectancy at birth in each country (Pearson's  $r = -0.25$ ,  $P = 0.008$ ) (**Fig. 2A**). Furthermore, the richness (Wilcoxon rank-sum test,  $P = 0.003$ ) and relative abundance (Wilcoxon rank-sum test,  $P = 0.030$ ) of HPB in the natural communities of low- and middle-income countries (LMICs) were significantly greater than those in high-income countries (HICs) (**Fig. 2B and fig. S3**). Similarly, the richness (Wilcoxon rank-sum test,  $P < 0.001$ ) and relative abundance (Wilcoxon rank-sum test,  $P = 0.002$ ) of HPB in countries with high human development levels were significantly greater than those in countries with medium and low human development levels (**Fig. 2C and fig. S3**). From a national perspective, the richness of HPB was significantly negatively correlated with Human Development Index (HDI, Pearson's  $r = -0.26$ ,  $P = 0.007$ ) and urban population (Pearson's  $r = -0.22$ ,  $P = 0.015$ ), whereas significantly positively correlated with Global Multidimensional Population Index (MPI, Pearson's  $r = 0.38$ ,  $P = 0.003$ ) and mortality rate per 100,000 by pathogen (Pearson's  $r = 0.28$ ,  $P = 0.002$ ) (**Fig. 2, D to G**). Consequently, socioeconomic factors such as poverty and low urban population might exacerbate the spread of HPB in the natural environment.

HPB exhibited an uneven distribution within natural environments, comprising a low number of high-abundance abundant taxa (species with a relative sequence abundance  $\geq 0.1\%$  across all samples of a habitat) and a high number of low-abundance rare taxa (species with a relative sequence abundance  $< 0.001\%$  across all samples of a habitat) (**fig. S4A**). Across various habitats, the proportion of rare taxa in HPB ranged from 70.1% (bird) to 94.2% (tundra), whereas the highest proportion of abundant taxa was only 3.2% (livestock). In 11 of these habitats, there were no HPB classified as abundant taxa. Furthermore, there were significant negative correlations between the richness (Pearson's  $r = -0.86$ ,  $P < 0.0001$ ) and relative abundance (Pearson's  $r = -0.86$ ,  $P < 0.0001$ ) of HPB and the proportion of rare taxa (**fig. S4, B and C**). Given that HPB in the environment are predominantly rare taxa, enhancing the sequencing depth could boost the detection rate of HPB (**fig. S4D**).

In sharp contrast to the rarity of relative abundance, HPB were mostly widely distributed globally (**fig. S5**). A total of 94.2% of the HPB species were shared among habitats, and 31.6% of the HPB species were present in all 26 studied habitats (**Fig. 2H**). The number of resistant drugs in HPB species was significantly positively correlated with both the average detection rate (Pearson's  $r = 0.27$ ,  $P < 0.0001$ ) and average niche breadth (Pearson's  $r = 0.13$ ,  $P = 0.018$ ) in various habitats (**Fig. 2, I and J**). Overall, HPB primarily constitute rare taxa, yet they are distributed across different habitats in natural environments.

## Global distribution of HPB

To determine the global patterns of HPB richness and abundance, we selected microbial communities with location and environmental information from global samples, excluding data related to oceans and humans for machine learning. Using sample datasets and global covariates (**table S3**), we constructed random forest models to

155 predict the global patterns of HPB richness and abundance. To avoid multicollinearity  
156 during model construction, we estimated the variance inflation factor (VIF) for the  
157 covariates and retained those with a VIF lower than 10. Based on 10-fold cross-  
158 validation, following feature selection and hyperparameter tuning, we identified the  
159 optimal feature set consisting of 37 covariates for model construction (**fig. S6 and table**  
160 **S4**).

161 Using random forest models, we predicted the richness of HPB at the global scale and  
162 mapped its distribution at a resolution of  $0.167^\circ$  (**Fig. 3A**). The prediction results  
163 indicated that HPB richness varied between 1.85 and 27.75 (mean: 9.10; median: 8.80).  
164 From a regional perspective, areas with frequent human activities (parts of East Asia),  
165 higher temperatures and radiation (parts of Africa and the Middle East), or greater  
166 precipitation (Southeast Asia, Central America), exhibited high HPB richness. HPB  
167 richness was particularly high in the Indian subcontinent, where human activities and  
168 temperatures are high. Conversely, regions with lower temperatures and precipitation,  
169 and less anthropogenic activity, such as Siberia, Canada, and the Qinghai-Tibetan  
170 Plateau, exhibited lower HPB richness. The hotspots of HPB relative abundance  
171 differed from those of richness but exhibited similar latitudinal trends, both showing a  
172 decreasing trend from low latitudes to high latitudes (**Fig. 3B and fig. S7**). In addition,  
173 after removing common commensal and opportunistic pathogenic bacteria, such as  
174 *Escherichia coli*, *Salmonella enterica*, and *Faecalibacterium prausnitzii*, we found that  
175 the global distribution and latitudinal trends of HPB richness and abundance were  
176 consistent with those without their removal (**fig. S8**).

177 The global distribution map of HPB suggested that climate factors and anthropogenic  
178 activities might have a profound impact on the richness of HPB. We categorized the  
179 variables utilized for model construction into several groups, such as climate factors  
180 and anthropogenic factors, and assessed their relative importance in predicting HPB  
181 richness (**Fig. 3, C and D**). The findings emphasized the significance of climate and  
182 anthropogenic activities as primary drivers of HPB richness: climate factors contain the  
183 greatest amount of model importance (44.2%), where temperature and precipitation  
184 variables each account for nearly 12%, and radiation and moisture variables each  
185 contribute more than 5%. Moreover, anthropogenic factors account for over 30% of  
186 model importance. This finding indicated that climate and anthropogenic factors, as the  
187 two major categories of variables, were responsible for nearly 80% to shaping HPB  
188 richness at the spatial scale. Moreover, some spatial variables, such as longitude,  
189 latitude, and elevation, also had an impact on the global distribution of HPB richness.  
190 Climate has been proven to be a critical factor determining the global distribution of  
191 fungi and plant-beneficial bacteria (24-28), and our findings highlighted the importance  
192 of climate factors in determining the richness of HPB. Additionally, the findings  
193 indicated that anthropogenic factors were also the primary factors affecting the global  
194 pattern of HPB richness, which could be attributed to human activities promoting the  
195 dissemination of HPB across different regions, consequently enhancing their richness.

196 **Global richness of HPB under future climate change scenarios**

197 The impact of climate change on the distribution of HPB remains largely uncertain.

198 Therefore, we simulated and predicted the richness of HPB by the end of this century  
199 (2081-2100) under four future climate scenarios (shared socioeconomic pathway (SSP)  
200 126, sustainability; SSP245, middle of the road; SSP370, regional rivalry; and SSP585,  
201 fossil-fuelled development).

202 First, we applied multivariate environmental similarity surface (MESS) analysis across  
203 the locations of the samples, and the results showed that, except for specific regions  
204 such as parts of Antarctica and the Sahara Desert, the samples used for prediction  
205 exhibited high extrapolation reliability for other regions (**fig. S9**). Through random  
206 forest modeling, we projected the global pattern of HPB richness by the end of this  
207 century under four scenarios: SSP126, SSP245, SSP370, and SSP585 (**Fig. 4A**). The  
208 findings revealed that HPB richness would increase across all the scenarios, with a  
209 greater increase observed as more climate change. Specifically, under the SSP126,  
210 SSP245, SSP370, and SSP585 scenarios, HPB richness increased by 11.7%, 16.8%,  
211 21.5%, and 26.6%, respectively (**Fig. 4, B and C**). This indicated that in scenarios of  
212 unsustainable development, the richness of HPB might be promoted. Similarly, a  
213 comparable trend was observed in the relative abundance of HPB (**fig. S10**). Except for  
214 certain regions of India, Africa, the Qinghai-Tibetan Plateau, and South America, where  
215 HPB richness declined, more than 60% of the areas exhibited upward trends across all  
216 the climate scenarios. In terms of latitudinal distribution, with the exception of the  
217 Southern Hemisphere midlatitude region, which experienced more fluctuations, HPB  
218 richness was expected to increase in almost all other regions, particularly in the  
219 Northern Hemisphere midlatitude region. After removing common commensal and  
220 opportunistic pathogenic bacteria, we evaluated the distribution patterns of remaining  
221 HPB richness and abundance under future climate scenarios (**fig. S11**). The results  
222 showed a similar trend of change.

223 Considering the various continents, HPB richness tended to increase across all  
224 continents, with the exception of Antarctica. The increase in HPB richness was more  
225 pronounced in continents such as Oceania and North America, compared to Africa (**fig.**  
226 **S12A**). Furthermore, variations in HPB richness were observed across regions with  
227 different income levels. The results revealed that the magnitude of the increase in HPB  
228 richness was significantly greater in "High income" and "Upper middle income" regions  
229 than in "Lower middle income" and "Low income" regions (**Fig. 4D**). Similarly, the  
230 findings related to HDI revealed that the magnitude of the increase in HPB richness in  
231 areas with high human development levels was significantly greater than that in areas  
232 with medium or low human development levels (**fig. S12B**). These findings indicated  
233 that, compared to those in regions with lower development levels, the magnitude of the  
234 increase in HPB richness in regions with higher development levels was more strongly  
235 influenced by climate change.

236 The maximum entropy model has been extensively applied to forecast the species  
237 distribution probability of diverse organisms at the global scale (24, 29, 30). Using this  
238 model, we evaluated the global invasion risk of HPB under current and different future  
239 climate scenarios (**Fig. 4E**). Under all the climate scenarios, East Asia, Europe, eastern  
240 North America, southern South America, and eastern Australia faced high invasion risks.

241 Although certain regions within these areas may experience a reduction in invasion risk  
242 in the future. Under various climate scenarios, the elevated invasion risks for SSP370  
243 (4.0%) and SSP585 (4.5%) were greater, whereas more sustainable scenarios (SSP126  
244 and SSP245) exhibited increases of 2.6% and 3.2%, respectively (fig. S13). The areas  
245 of increased invasion risk were primarily concentrated in the Northern Hemisphere  
246 midlatitude regions. Our findings highlighted the need for sustainable development to  
247 limit future HPB invasions, particularly in the Northern Hemisphere mid- and high-  
248 latitude regions.

249

## 250 Discussion

251 Current infections remain the leading cause of death globally, and the prevalence of  
252 pathogenic bacteria in the environment has led to severe human diseases (11, 22).  
253 According to the latest list released by the World Health Organization (WHO), the  
254 number of pathogens that might trigger the next pandemic has increased to over 30,  
255 including five bacteria (31, 32). To more effectively address public health challenges,  
256 the concept of "One Health" has been proposed, which emphasizes the interdependence  
257 of human, animal, plant, and environmental health, aiming to sustainably balance and  
258 optimize health (14). Although numerous studies have revealed the intimate connection  
259 between specific environments and HPB (15-19), there remains a lack of surveillance  
260 of pathogenic bacteria in the environment on a global scale. In this study, we conducted  
261 detection for potential HPB in more than one million microbial communities from  
262 various habitats including animal, plant, soil, and aquatic globally, and ultimately  
263 detected HPB in nearly 90% of the communities. The identified HPB were from 9 phyla,  
264 with 59% of the species belonging to Pseudomonadota and Bacillota, which contain *E.*  
265 *coli*, *Staphylococcus aureus*, *Streptococcus pneumoniae*, *Klebsiella pneumoniae*, and  
266 *Pseudomonas aeruginosa* that are responsible for mass deaths caused by bacteria (11).  
267 Focusing on HPB with pandemic potential can help prevent public health emergencies  
268 of international concern. Studies have shown that HPB can exploit various habitats and  
269 exist in multiple environments, among which environments influenced by human  
270 activities are more likely to harbor HPB (33, 34). This observation is consistent with  
271 our results, which emphasize that the natural environment can serve as a reservoir for  
272 HPB and that environments with closer relationships with humans typically harbor  
273 more HPB. We also found that the number of resistant drugs in HPB species was  
274 correlated with the detection rate and niche breadth, suggesting that the transmission of  
275 HPB between environments may be promoted by antibiotic resistance. These findings  
276 support the hypothesis that anthropogenic activities facilitate the transmission of  
277 pathogens, reinforcing the concept of "One Health" (35, 36).

278 Considerable variation exists in the burden of bacterial infections across different  
279 regions, with LMICs bearing the greatest burden of infectious diseases (11, 37, 38). Our  
280 results also reflected a correlation between the distribution of HPB and development  
281 level. In regions with higher development levels, HPB have lower detection rates,  
282 richness, and relative abundance, whereas in regions with lower development levels,

283 these indicators are higher. Regions with higher development levels are associated with  
284 more wealth, which can achieve more urban population and improve access to  
285 sanitation, clean water, and health care, thereby increasing life expectancy and reducing  
286 the mortality rate (13). Socioeconomic drivers play an underappreciated role in the  
287 spread of HPB, and poverty and other factors might exacerbate this process. These  
288 results support the disease-driven poverty trap hypothesis (39-41), positing that poor  
289 people may be ensnared in a reinforced cycle of poverty and disease, in which they are  
290 more susceptible to infections mediated by the environment. Our findings highlight the  
291 pressing need for better HPB surveillance and control efforts in underdeveloped regions.  
292 Although medical advances in the twenty-first century have promoted progress in  
293 human health, inequalities between different countries still exist (42). Therefore, there  
294 is an urgent need to increase access to medical services in areas with lower development  
295 levels.

296 In addition to dominant retrospective analysis, more forward-looking research is needed  
297 to address potential future changes. Climate change profoundly affects and alters  
298 microorganisms on Earth (43-45). Climate extremes disrupt fungal-bacterial  
299 interactions, thereby destabilizing soil microbial communities (46). Studies have shown  
300 that by the end of this century, fossil-fuel-dependent scenarios could lead to a significant  
301 decrease of global plant-beneficial bacteria abundance in soils, whereas the diversity  
302 and invasive potential of phytopathogenic fungi will increase globally (24, 28).  
303 Simultaneously, climate change is having a profound impact on human health, with  
304 more than half of human pathogenic diseases being aggravated (5). The profound  
305 impact of climate change on HPB has been established: on the one hand, climate change  
306 can directly affect specific aspects of pathogens, promoting climate suitability for  
307 reproduction, accelerating the life cycle, and increasing virulence (5); on the other hand,  
308 climate change indirectly influences pathogens by affecting the reproduction, survival,  
309 and geographic distribution of vectors (47). Changes in climate have facilitated cross-  
310 species transmission of viruses (9). The adaptation of microorganisms to higher  
311 temperatures may lead to the possibility of previously unrecognized infectious diseases.  
312 The increase in heat tolerance of fungi with pathogenic potential, driven by global  
313 warming, may lead to the emergence of new fungal diseases (10). Our findings  
314 indicated that under future climate scenarios, the richness, relative abundance, and  
315 invasion risk of HPB would show upward, with greater increases observed as the  
316 sustainability of development decreases. Compared to those in the "Lower middle  
317 income" and "Low income" regions, the magnitude of the increase in HPB richness was  
318 significantly greater in the "High income" and "Upper middle income" regions.  
319 Although regions with lower levels of development currently have higher levels of HPB  
320 richness, relative abundance, and bacterial infection burden, climate change also has  
321 impact on regions with higher levels of development. To limit the role of climate change  
322 in increasing pathogen spillover risk, we must reduce greenhouse gas emissions and  
323 pursue sustainable development. Additionally, the risk of HPB is shared globally, thus  
324 humanity should unite to assist underdeveloped areas in accessing healthcare and  
325 improving medical conditions.

326 This study provides an omnidirectional understanding on the global biogeography of

327 HPB and the impact of climate change on their distribution. It is important to  
328 acknowledge that there remain limitations of our research. This study is based on  
329 mapping HPB genome to OTUs, which may mask the complexity in HPB. By  
330 attempting to remove common commensal and opportunistic pathogenic bacteria such  
331 as *E. coli*, we found that our conclusions remain unchanged. In addition, the  $R^2$  of our  
332 machine learning models is less than 0.5, indicating a certain lack of interpretability.  
333 However, considering that we used data from over 10,000 nonredundant locations for  
334 machine learning, our models perform robustly. Moreover, the current sample  
335 distribution is uneven due to sampling constraints, with sampling points mainly  
336 concentrated in the Northern Hemisphere and insufficient sampling in the Southern  
337 Hemisphere. Moreover, available data for LMICs remain scarce, despite these countries  
338 bearing a greater burden of bacterial infections. Therefore, future efforts should  
339 prioritize sampling and research in LMICs. Furthermore, projections for future HPB  
340 richness depend on the predominant role of climate covariates in current condition. If  
341 there are changes in the key drivers for HPB richness under future climate scenarios,  
342 the predictions need to be revised.

343 In conclusion, we conducted large-scale HPB identification of microbial communities  
344 from global ecosystems, identified the taxonomic composition and distribution of  
345 potential HPB, and determined their widespread presence in the natural environment.  
346 Furthermore, we observed that HPB varied among different habitats and regions with  
347 varying development levels, with human activities promoting the dispersal of HPB  
348 between environments. Using modeling methods, we created global maps detailing the  
349 distribution of HPB richness and relative abundance, assessed the impact of climate  
350 change on the distribution of pathogenic bacteria, and found that unsustainable  
351 development could exacerbate the dispersal of HPB. The findings indicated the intimate  
352 connection between human health and the ecological environment, supporting the  
353 concept of "One Health". Additionally, we found that human activities and climate  
354 change could profoundly affect the distribution, richness, and dispersal of HPB in the  
355 environment, highlighting the necessity and urgency of reducing greenhouse gas  
356 emissions and assisting LMICs in improving medical conditions.

357

## 358 Materials and Methods

### 359 Data collection of human pathogenic bacteria (HPB)

360 The Global Catalogue of Pathogens (gcPathogen) (23) is a comprehensive genomic  
361 resource containing known human pathogens isolated from infected patients, animal  
362 hosts, and the environment, aimed at supporting scientific research on pathogens and  
363 public health surveillance. Guided by institutions such as the World Health  
364 Organization (WHO), gcPathogen has compiled a list of human pathogens, including  
365 bacteria, fungi, viruses, and parasites. All sequences for the pathogens were obtained  
366 from the genomic database of the National Center for Biotechnology Information  
367 (NCBI), and the relevant metadata were retrieved from BioSamples and manually

368 curated. This study collected genomic data of HPB from 499 species and extracted  
369 information on biosafety levels, number of resistant drugs, and disease for each  
370 pathogenic bacterium from the gcPathogen (as of 10 April 2024).

### 371 **Data collection of microbial communities**

372 The Microbe Atlas Project (MAP) (48) summarized and organized a large number of  
373 sequenced microbial communities, aiming to provide additional perspectives for  
374 microbial ecology. The MAP retrieved metadata summary files from the NCBI  
375 Sequence Read Archive (SRA) database and searched for keywords such as  
376 "metagenomic", "microb\*", "bacteria", or "archaea". The raw data were downloaded  
377 and quality filtered for all selected sequencing runs. Then, the MAPseq tool was used  
378 to assign taxonomic and operational taxonomic unit (OTU) labels to the filtered reads  
379 based on different 16S ribosomal RNA (rRNA) gene identity cutoffs (90%, 96%, 97%,  
380 98%, 99%). This study extracted data with OTUs defined at 99% sequence identity,  
381 filtered out samples with total ribosomal RNA reads less than 10,000 and number of  
382 OTUs in the sample less than 20, and removed samples related to humans.

383 Based on the metadata obtained from MAP, we categorized the samples into four major  
384 categories of habitats: animal, plant, soil, and aquatic, which were further classified into  
385 26 distinct microbial habitats. Animal-associated habitats were categorized into six  
386 types: livestock (including pig, cattle, sheep, and goat), bird (such as sparrow), insecta  
387 (such as fruitfly), pet (including cat and dog), fish (such as zebrafish), and primate (such  
388 as chimpanzee). Plant-associated habitats were divided into four types: rhizosphere,  
389 leaf, wood, and seed. The soil habitats were classified into eight types: field, forest,  
390 agricultural, farm, shrub, peatland, desert, and tundra. The aquatic habitats were  
391 categorized into eight types: marine (marine, ocean, and sea were all assigned this type),  
392 sediment, river, waste water, lake, estuary, reservoir, and groundwater. Anthropogenic  
393 habitats represent habitats closely associated with humans, including: pet, livestock,  
394 primate, farm, agricultural, and waste water.

### 395 **Mapping the genomes of HPB to OTUs**

396 We predicted the 16S rRNA gene sequences in HPB genomes collected from the  
397 gcPathogen using Barrnap v.0.9 (49) with default parameters. Using the MAPseq  
398 v.2.1.1 tool, we mapped the predicted 16S rRNA gene sequences to MAPref v.3.0 (48),  
399 which contains 1,360,792 OTU sequences. The outputs provided confidence levels on  
400 the mapping between 16S rRNA gene sequences and OTU sequences, and the mapping  
401 results that met the following two conditions were chosen: (i) confidence level  $\geq 0.5$ ,  
402 matching length of 16S rRNA gene sequences and OTU sequences  $\geq 800$ , providing  
403 the best match for genomes mapped to multiple OTUs based on the majority principle  
404 (proportion  $\geq 50\%$ ); (ii) confidence level  $\geq 0.98$ , matching length between 16S rRNA  
405 gene sequences and OTU sequences  $\geq 800$ , providing the best match for genomes  
406 mapped to multiple OTUs based on the optimal principle (proportion  $< 50\%$ , but  
407 maximum). Moreover, the outputs provided taxonomic labels for each OTU, which we  
408 compared with the taxonomic information obtained based on the assembly accession  
409 number to remove abnormal results. Ultimately, we identified 733 HPB OTUs within

410 1,066,584 sequenced microbial communities.

411 On the basis of the OTU tables retrieved from MAP, we calculated the richness and  
412 abundance of pathogenic bacteria in each microbial community, respectively. The  
413 richness of HPB was determined based on the OTU number of HPB in the microbial  
414 communities, while the abundance of HPB was calculated as follows:

$$415 \quad PA = \text{sum}(OR)/TR \times 10^6$$

416 where PA is the abundance of HPB, OR represents reads of HPB OTUs, and TR is total  
417 reads of microbial communities.

#### 418 **Acquisition of socioeconomic factors**

419 We obtained data on Human Development Index (HDI) and Global Multidimensional  
420 Population Index (MPI) from the United Nations (<https://hdr.undp.org/>), with HDI from  
421 2024 and MPI from 2023. Life expectancy at birth, urban population, and income level  
422 data were collected from the World Bank (<https://www.worldbank.org/>), with life  
423 expectancy at birth and urban population from 2022 and income level data from the  
424 2024 fiscal year. The mortality rate per 100,000 by pathogen in 2019 was derived from  
425 a study conducted in 2022 (11).

#### 426 **Niche breadth of HPB**

427 Niche breadth is a notable characteristic that affects the relative importance of  
428 determinism and stochasticity in community assembly (50), reflecting differences in  
429 the adaptability of different species to various environmental conditions. Levins  
430 proposed evaluating the niche breadth of species by calculating the evenness of species  
431 distribution under various resource states. Levins' niche breadth index (B) was  
432 calculated as follows:

$$433 \quad B_j = 1 / \sum_{i=1}^N P_{ij}^2$$

434 where  $B_j$  represents the niche breadth of species j,  $P_{ij}$  represents the proportion of  
435 species j in resource state i, and N is the total number of resource states. The range of  
436  $B_j$  is from 1 to N. Because of different sampling times, the number of resource states  
437 also varies, resulting in different ranges of  $B_j$ . For convenience of comparison, it is  
438 necessary to standardize  $B_j$  to a range from 0 to 1. Levins' standardized niche breadth  
439 ( $B_A$ ) was calculated as follows:

$$440 \quad B_A = (B - 1)/(N - 1)$$

441 Finally, we calculated the average  $B_A$  of each species ( $B_{avg}$ ) as an indicator of niche  
442 breadth.

#### 443 **Acquisition of gridded covariates**

444 We downloaded historical data for 19 bioclimatic variables from WorldClim,  
445 representing the average for the years 1970-2000. Meanwhile, we also extracted future  
446 (2080-2100) climate data on these bioclimatic variables. There are four Shared Socio-

447 economic Pathways (SSP) in future climate data: SSP126: sustainability; SSP245:  
448 middle of the road; SSP370: regional rivalry; and SSP585: fossil-fuelled development.  
449 Then, we obtained additional 21 bioclimatic variables from CliMond. Furthermore, we  
450 retrieved global maps related to climate variables from other databases. Anthropogenic  
451 variables were collected from CGIAR-CSI, DRYAD, and SEDAC, whereas soil  
452 properties were derived from SoilGrids. In addition, elevation data was collected from  
453 GMTED2010, biomass data was obtained from CDIAC, and plant functional type data  
454 was acquired from GCAM. The covariates were categorized into 9 types: anthropogenic,  
455 temperature, radiation, precipitation, moisture, other climatic variables, soil properties,  
456 spatial, and others. Detailed information on the covariates was presented in table S3. To  
457 obtain maps of the same resolution, we resampled all the datasets to match the same  
458 resolution by using the nearest neighbor method.

#### 459 **Random forest modeling**

460 First, we processed the data from MAP, selected samples with location information, and  
461 excluded data related to oceans and humans. The covariates corresponding to each  
462 sampling location were extracted through ArcGIS Pro. Duplicates were removed from  
463 samples with the same coordinates, and the richness and abundance of HPB at each  
464 location were calculated by averaging. To mitigate spatial autocorrelation, we retained  
465 only one sample within 10 meters of each other. Additionally, we employed the  
466 blockCV (51) package, which allows for separation of data spatially, ensuring the  
467 creation of training and testing sets that are spatially separate.

468 Then, the global patterns of HPB richness and abundance were estimated using random  
469 forest models. First, to avoid multicollinearity, we evaluated the variance inflation  
470 factor (VIF) of the variables and removed covariates with a VIF greater than 10. Then,  
471 the recursive feature elimination algorithm was used to determine the best combination  
472 of features. Afterward, we conducted hyperparameter tuning with the optimal features  
473 using grid search to identify the optimal combination of hyperparameters. Both of these  
474 procedures were performed on the basis of 10-fold cross-validation, which minimizes  
475 the problem of model overfitting. The 10-fold cross-validation  $R^2$  was used to assess  
476 the performance of the model. Finally, we validated our model on the testing set to  
477 evaluate its predictive ability on untrained data (**fig. S14**).

478 Finally, we set 10 different random seeds to train 10 independent random forest models,  
479 calculated the average of 10 predictions as the final results, and calculated the  
480 coefficients of variation of the 10 predicted results to evaluate the uncertainty of the  
481 model (**fig. S14**).

482 The importance of each variable was also determined through machine learning to  
483 evaluate the key factors affecting the global distribution of HPB. We estimated the  
484 importance of the chosen variables by the function for variable importance measures in  
485 the randomForest (52) package of R. For the convenience of comparison, we  
486 standardized the importance of these variables on a scale of 0-100% to obtain their  
487 relative importance (**table S4 and table S5**).

488 To verify our results, we used spatial cross-validation with the blockCV package, which

489 offers a range of functions for generating k-fold cross-validation to ensure spatial  
490 separation. Based on spatial cross-validation, we performed feature selection and  
491 hyperparameter tuning to construct models that predict the global patterns of HPB  
492 richness and abundance (**fig. S15**).

#### 493 **Future richness and abundance projections**

494 A multivariate environmental similarity surface (MESS) analysis was conducted on the  
495 locations of the samples to evaluate the extrapolation reliability of HPB. Using the  
496 random forest algorithm, nine-tenths of the samples were allocated as the training  
497 dataset for the model, whereas one-tenth served as the testing set. The dataset used for  
498 future projections has also been removed samples with close distances and divided into  
499 spatially separate training and testing sets. Based on historical data of 19 bioclimatic  
500 variables sourced from WorldClim, the global distribution of HPB under the current  
501 climate was estimated. The 10-fold cross-validation  $R^2$  was used to assess the  
502 performance of the model, and the testing set was used to evaluate its predictive ability  
503 on untrained data (**fig. S16**). Using the established model and based on future (2080-  
504 2100) climate data of 19 bioclimatic variables, we predicted the potential richness and  
505 abundance of HPB under various future climate scenarios. Each future climate scenario  
506 contains multiple different CMIP6 downscaled global climate models (GCMs, **table**  
507 **S6**), and the projections of different GCMs were averaged. For future projections of  
508 HPB richness and abundance, we also used spatial cross-validation to confirm the  
509 findings (**fig. S17**).

#### 510 **Future invasion risk projection**

511 Using Maxent software, the global invasion risks of HPB under current and future  
512 climate conditions were assessed through the maximum entropy model (53). This model  
513 has been extensively utilized for predicting the probability of species distributions of  
514 various organisms across the globe. The outcomes represent the predicted probability  
515 of suitable conditions, with higher values corresponding to a high likelihood of suitable  
516 conditions for HPB and lower values corresponding to a low likelihood. In this study,  
517 the prediction probability was considered as invasion risk of HPB. First, the occurrence  
518 data of HPB, along with 19 current bioclimatic variables, were imported into Maxent  
519 software to generate the global distribution probability of HPB, which reflects the  
520 invasion risk. We subsequently projected the future invasion risk of HPB by the end of  
521 this century (2081-2100) under four future climate scenarios and assessed the changes  
522 in invasion risk relative to the current climate conditions. The following settings were  
523 used to run the model: feature classes = auto, replicates = 10, replicated run type =  
524 Crossvalidate, maximum iterations = 500, convergence threshold = 0.00001.

#### 525 **Statistical analyses**

526 The data analysis was mainly conducted using R (version 4.3.3). Through the caret (54)  
527 and randomForest (52) packages, the recursive feature elimination algorithm,  
528 hyperparameter tuning, and calculation of the relative importance of variables were  
529 performed. The partial results were visualized by the ggplot2 (55) package. ArcGIS Pro  
530 was used to extract covariates corresponding to location points and visualize the global

531 distribution of HPB.

532

533 **References**

- 534 1. A. Costello, M. Abbas, A. Allen, S. Ball, S. Bell, R. Bellamy, S. Friel, N. Groce, A.  
535 Johnson, M. Kett, Managing the health effects of climate change: Lancet and  
536 University College London Institute for Global Health Commission. *Lancet* **373**,  
537 1693-1733 (2009).
- 538 2. D. Campbell-Lendrum, T. Neville, C. Schweizer, M. Neira, Climate change and  
539 health: three grand challenges. *Nat Med* **29**, 1631-1638 (2023).
- 540 3. W. Cai, J. Fanzo, J. Glaser, R. Lowe, A. M. Lusambili, E. Marks, Views on climate  
541 change and health. *Nat Clim Chang* **14**, 419-423 (2024).
- 542 4. Talking about climate change and health. *Nat Clim Chang* **14**, 409 (2024).
- 543 5. C. Mora, T. McKenzie, I. M. Gaw, J. M. Dean, H. von Hammerstein, T. A. Knudson,  
544 R. O. Setter, C. Z. Smith, K. M. Webster, J. A. Patz, Over half of known human  
545 pathogenic diseases can be aggravated by climate change. *Nat Clim Chang* **12**, 869-  
546 875 (2022).
- 547 6. M. B. Mahon, A. Sack, O. A. Aleuy, C. Barbera, E. Brown, H. Buelow, D. J.  
548 Civitello, J. M. Cohen, L. A. de Wit, M. Forstchen, A meta-analysis on global  
549 change drivers and the risk of infectious disease. *Nature* **629**, 830-836 (2024).
- 550 7. Climate change exacerbates almost two-thirds of pathogenic diseases affecting  
551 humans. *Nat Clim Chang* **12**, 791-792 (2022).
- 552 8. Small organisms with big climate impact. *Nat Microbiol* **8**, 2213-2214 (2023).
- 553 9. C. J. Carlson, G. F. Albery, C. Merow, C. H. Trisos, C. M. Zipfel, E. A. Eskew, K.  
554 J. Olival, N. Ross, S. Bansal, Climate change increases cross-species viral  
555 transmission risk. *Nature* **607**, 555-562 (2022).
- 556 10. A. Casadevall, Global warming could drive the emergence of new fungal pathogens.  
557 *Nat Microbiol* **8**, 2217-2219 (2023).
- 558 11. K. S. Ikuta, L. R. Swetschinski, G. R. Aguilar, F. Sharara, T. Mestrovic, A. P. Gray,  
559 N. D. Weaver, E. E. Wool, C. Han, A. G. Hayoon, Global mortality associated with  
560 33 bacterial pathogens in 2019: a systematic analysis for the Global Burden of  
561 Disease Study 2019. *Lancet* **400**, 2221-2248 (2022).
- 562 12. I. N. Okeke, M. E. de Kraker, T. P. Van Boeckel, C. K. Kumar, H. Schmitt, A. C.  
563 Gales, S. Bertagnolio, M. Sharland, R. Laxminarayan, The scope of the  
564 antimicrobial resistance challenge. *Lancet* **403**, 2426-2438 (2024).
- 565 13. S. H. Sokolow, N. Nova, I. J. Jones, C. L. Wood, K. D. Lafferty, A. Garchitorena,  
566 S. R. Hopkins, A. J. Lund, A. J. MacDonald, C. LeBoa, Ecological and  
567 socioeconomic factors associated with the human burden of environmentally  
568 mediated pathogens: a global analysis. *Lancet Planet Health* **6**, e870-e879 (2022).
- 569 14. Tripartite and UNEP support OHHEP's definition of "One Health". *WHO*, (2021).
- 570 15. B. K. Singh, Z.-Z. Yan, M. Whittaker, R. Vargas, A. Abdelfattah, Soil microbiomes  
571 must be explicitly included in One Health policy. *Nat Microbiol* **8**, 1367-1372  
572 (2023).
- 573 16. S. Banerjee, M. G. Van Der Heijden, Soil microbiomes and one health. *Nat Rev*

- 574                   *Microbiol* **21**, 6-20 (2023).
- 575     17. A. G. Shaw, C. Troman, J. O. Akello, K. M. O'reilly, J. Gauld, S. Grow, N. Grassly,  
576       D. Steele, D. Blazes, S. Kumar, Defining a research agenda for environmental  
577       wastewater surveillance of pathogens. *Nat Med* **29**, 2155-2157 (2023).
- 578     18. Y. Dong, Z. Jiang, Y. Hu, Y. Jiang, L. Tong, Y. Yu, J. Cheng, Y. He, J. Shi, Y. Wang,  
579       Pathogen contamination of groundwater systems and health risks. *Crit Rev Environ  
580       Sci Technol* **54**, 267-289 (2024).
- 581     19. L. Doni, J. Martinez-Urtaza, L. Vezzulli, Searching pathogenic bacteria in the rare  
582       biosphere of the ocean. *Curr Opin Biotechnol* **80**, 102894 (2023).
- 583     20. K. K. Ko, K. R. Chng, N. Nagarajan, Metagenomics-enabled microbial  
584       surveillance. *Nat Microbiol* **7**, 486-496 (2022).
- 585     21. J. L. Gardy, N. J. Loman, Towards a genomics-informed, real-time, global  
586       pathogen surveillance system. *Nat Rev Genet* **19**, 9-20 (2018).
- 587     22. D. Zhu, Y. Zhang, Y.-G. Zhu, Human pathogens in the soil ecosystem: Occurrence,  
588       dispersal, and study method. *Curr Opin Environ Sci Health* **33**, 100471 (2023).
- 589     23. C. Guo, Q. Chen, G. Fan, Y. Sun, J. Nie, Z. Shen, Z. Meng, Y. Zhou, S. Li, S. Wang,  
590       gcPathogen: a comprehensive genomic resource of human pathogens for public  
591       health. *Nucleic Acids Res* **52**, D714-D723 (2024).
- 592     24. P. Li, L. Tedersoo, T. W. Crowther, B. Wang, Y. Shi, L. Kuang, T. Li, M. Wu, M.  
593       Liu, L. Luan, Global diversity and biogeography of potential phytopathogenic  
594       fungi in a changing world. *Nat Commun* **14**, 6482 (2023).
- 595     25. L. Tedersoo, M. Bahram, S. Põlme, U. Kõljalg, N. S. Yorou, R. Wijesundera, L. V.  
596       Ruiz, A. M. Vasco-Palacios, P. Q. Thu, A. Suija, Global diversity and geography of  
597       soil fungi. *Science* **346**, 1256688 (2014).
- 598     26. T. Větrovský, P. Kohout, M. Kopecký, A. Machac, M. Man, B. D. Bahnmann, V.  
599       Brabcová, J. Choi, L. Meszárošová, Z. R. Human, A meta-analysis of global fungal  
600       distribution reveals climate-driven patterns. *Nat Commun* **10**, 5142 (2019).
- 601     27. M. Delgado-Baquerizo, C. A. Guerra, C. Cano-Díaz, E. Egidi, J.-T. Wang, N.  
602       Eisenhauer, B. K. Singh, F. T. Maestre, The proportion of soil-borne pathogens  
603       increases with warming at the global scale. *Nat Clim Chang* **10**, 550-554 (2020).
- 604     28. P. Li, L. Tedersoo, T. W. Crowther, A. J. Dumbrell, F. Dini-Andreote, M. Bahram,  
605       L. Kuang, T. Li, M. Wu, Y. Jiang, Fossil-fuel-dependent scenarios could lead to a  
606       significant decline of global plant-beneficial bacteria abundance in soils by 2100.  
607       *Nat Food* **4**, 996-1006 (2023).
- 608     29. R. Tingley, M. Vallinoto, F. Sequeira, M. R. Kearney, Realized niche shift during a  
609       global biological invasion. *Proc Natl Acad Sci U S A* **111**, 10233-10238 (2014).
- 610     30. L. Zhao, J. Li, X. Cui, N. Jia, J. Wei, L. Xia, H. Wang, Y. Zhou, Q. Wang, X. Liu,  
611       C. Yin, Y. Pan, H. Wen, Q. Wang, F. Xue, Y. Sun, J. Jiang, S. Li, W. Cao,  
612       Distribution of *Haemaphysalis longicornis* and associated pathogens: analysis of  
613       pooled data from a China field survey and global published data. *Lancet Planet  
614       Health* **4**, e320-e329 (2020).
- 615     31. S. Mallapaty, The pathogens that could spark the next pandemic. *Nature* **632**, 488  
616       (2024).
- 617     32. Pathogens prioritization: a scientific framework for epidemic and pandemic

- 618 research preparedness. *WHO*, (2024).
- 619 33. C. Bonneau, L. A. Weinert, B. Kuijper, Understanding the emergence of bacterial  
620 pathogens in novel hosts. *Philos Trans R Soc Lond B Biol Sci* **374**, 20180328 (2019).
- 621 34. T. Li, K. Feng, S. Wang, X. Yang, X. Peng, Q. Tu, Y. Deng, Beyond water and soil:  
622 Air emerges as a major reservoir of human pathogens. *Environ Int* **190**, 108869  
623 (2024).
- 624 35. R. E. Baker, A. S. Mahmud, I. F. Miller, M. Rajeev, F. Rasambainarivo, B. L. Rice,  
625 S. Takahashi, A. J. Tatem, C. E. Wagner, L.-F. Wang, Infectious disease in an era  
626 of global change. *Nat Rev Microbiol* **20**, 193-205 (2022).
- 627 36. B. A. Jones, D. Grace, R. Kock, S. Alonso, J. Rushton, M. Y. Said, D. McKeever,  
628 F. Mutua, J. Young, J. McDermott, Zoonosis emergence linked to agricultural  
629 intensification and environmental change. *Proc Natl Acad Sci U S A* **110**, 8399-  
630 8404 (2013).
- 631 37. K. E. Rudd, S. C. Johnson, K. M. Agesa, K. A. Shackelford, D. Tsoi, D. R. Kievlan,  
632 D. V. Colombara, K. S. Ikuta, N. Kissoon, S. Finfer, Global, regional, and national  
633 sepsis incidence and mortality, 1990-2017: analysis for the Global Burden of  
634 Disease Study. *Lancet* **395**, 200-211 (2020).
- 635 38. A. E. Mather, M. W. Gilmour, S. W. Reid, N. P. French, Foodborne bacterial  
636 pathogens: genome-based approaches for enduring and emerging threats in a  
637 complex and changing world. *Nat Rev Microbiol* **22**, 543-555 (2024).
- 638 39. M. H. Bonds, A. P. Dobson, D. C. Keenan, Disease ecology, biodiversity, and the  
639 latitudinal gradient in income. *PLoS Biol* **10**, e1001456 (2012).
- 640 40. A. Garchitorena, S. Sokolow, B. Roche, C. Ngonghala, M. Jocque, A. Lund, M.  
641 Barry, E. Mordecai, G. Daily, J. Jones, Disease ecology, health and the environment:  
642 a framework to account for ecological and socio-economic drivers in the control of  
643 neglected tropical diseases. *Philos Trans R Soc Lond B Biol Sci* **372**, 20160128  
644 (2017).
- 645 41. M. H. Bonds, D. C. Keenan, P. Rohani, J. D. Sachs, Poverty trap formed by the  
646 ecology of infectious diseases. *Proc Biol Sci* **277**, 1185-1192 (2010).
- 647 42. P. J. Hotez, Globalists versus nationalists: Bridging the divide through blue marble  
648 health. *PLoS Negl Trop Dis* **13**, e0007156 (2019).
- 649 43. European Food Safety Authority, A. Maggiore, A. Afonso, F. Barrucci, G. D.  
650 Sanctis, Climate change as a driver of emerging risks for food and feed safety, plant,  
651 animal health and nutritional quality. *EFSA Supp Publ* **17**, 1881E (2020).
- 652 44. M. E. Morgado, C. Jiang, J. Zambrana, C. R. Upperman, C. Mitchell, M. Boyle, A.  
653 R. Sapkota, A. Sapkota, Climate change, extreme events, and increased risk of  
654 salmonellosis: foodborne diseases active surveillance network (FoodNet), 2004-  
655 2014. *Env Health* **20**, 105 (2021).
- 656 45. R. S. Hellberg, E. Chu, Effects of climate change on the persistence and dispersal  
657 of foodborne bacterial pathogens in the outdoor environment: A review. *Crit Rev  
658 Microbiol* **42**, 548-572 (2016).
- 659 46. J. Shi, M. P. Thakur, Climate extremes disrupt fungal-bacterial interactions. *Nat  
660 Microbiol* **8**, 2226-2229 (2023).
- 661 47. W. M. de Souza, S. C. Weaver, Effects of climate change and human activities on

- vector-borne diseases. *Nat Rev Microbiol* **22**, 476-491 (2024).
48. J. F. Matias Rodrigues, T. S. Schmidt, J. Tackmann, C. von Mering, MAPseq: highly efficient k-mer search with confidence estimates, for rRNA sequence analysis. *Bioinformatics* **33**, 3808-3810 (2017).
49. T. Seemann, barrnap 0.9: rapid ribosomal RNA prediction. (2018).
50. W. Wu, H.-P. Lu, A. Sastri, Y.-C. Yeh, G.-C. Gong, W.-C. Chou, C.-H. Hsieh, Contrasting the relative importance of species sorting and dispersal limitation in shaping marine bacterial versus protist communities. *ISME J* **12**, 485-494 (2018).
51. R. Valavi, J. Elith, J. J. Lahoz-Monfort, G. Guillera-Arroita, blockCV: An r package for generating spatially or environmentally separated folds for k-fold cross-validation of species distribution models. *Methods Ecol Evol* **10**, 225-232 (2019).
52. A. Liaw, M. Wiener, Classification and regression by randomForest. *R News* **2**, 18-22 (2002).
53. S. J. Phillips, M. Dudík, Modeling of species distributions with Maxent: new extensions and a comprehensive evaluation. *Ecography* **31**, 161-175 (2008).
54. M. Kuhn, Building predictive models in R using the caret package. *J Stat Softw* **28**, 1-26 (2008).
55. H. Wickam, ggplot2: elegant graphics for data analysis. *Springer-Verlag New York*, (2016).

681

## 682 Acknowledgments

683 **Funding:** This work was supported by the Science & Technology Fundamental  
684 Resources Investigation Program (2022FY101100 to Z.Z.), the National Natural  
685 Science Foundation of China (32270073 to Z.Z. and 32401327 to Y.L.), the Science  
686 Foundation for Youths of Shandong Province (ZR2022QC001 to Y.L.), and the Natural  
687 Science Foundation of Jiangsu Province (BK20230248 to Y.L.).

688 **Author contributions:** Writing-original draft: Y.G., Z.Z., Y.L., P.L., Y.J., and Y.-Z.L.  
689 Conceptualization: Y.G., Z.Z., Y.L., and Y.-Z.L. Investigation: Y.G., Z.Z., and Y.L.  
690 Writing-review and editing: Y.G., Z.Z., Y.L., P.L., J.S., Y.J., Z.P., and Y.-Z.L.  
691 Methodology: Y.G., Z.Z., and Y.L. Resources: Y.G., Z.Z., and Y.L. Funding acquisition:  
692 Z.Z. and Y.L. Data curation: Y.G., Z.Z., Y.L., and J.S. Validation: Y.G., Z.Z., Y.L., P.L.,  
693 J.S., and Y.J. Supervision: Z.Z. and Y.L. Formal analysis: Y.G., Z.Z., Y.L., P.L., J.S., and  
694 Y.J. Software: Y.G., Z.Z., P.L., and J.S. Project administration: Z.Z. and Y.L.  
695 Visualization: Y.G., Z.Z., and Y.L.

696 **Competing interests:** Authors declare that they have no competing interests.

697 **Data and materials availability:** All data needed to evaluate the conclusions in the  
698 paper are present in the paper and/or the Supplementary Materials. All genomic data of  
699 HPB are available in the gcPathogen database (<https://nmdc.cn/gcpathogen/>). All  
700 microbial communities and samples are available in the MAP database  
701 (<https://microbeatlas.org/>). The socioeconomic factors used in the current study are  
702 available from the United Nations (<https://hdr.undp.org/>) and the World Bank  
703 (<https://www.worldbank.org/>). The current and future climate data are available from

704 WorldClim (<https://www.worldclim.org/>). Detailed information on the other covariates  
705 used in the current study is presented in table S3. Source data are provided with this  
706 paper. All the codes for machine learning and statistical analysis used in this study are  
707 available online at <https://doi.org/10.5061/dryad.msbcc2g82>.

708

709 **Supplementary Materials:**

710 **This PDF file includes:**

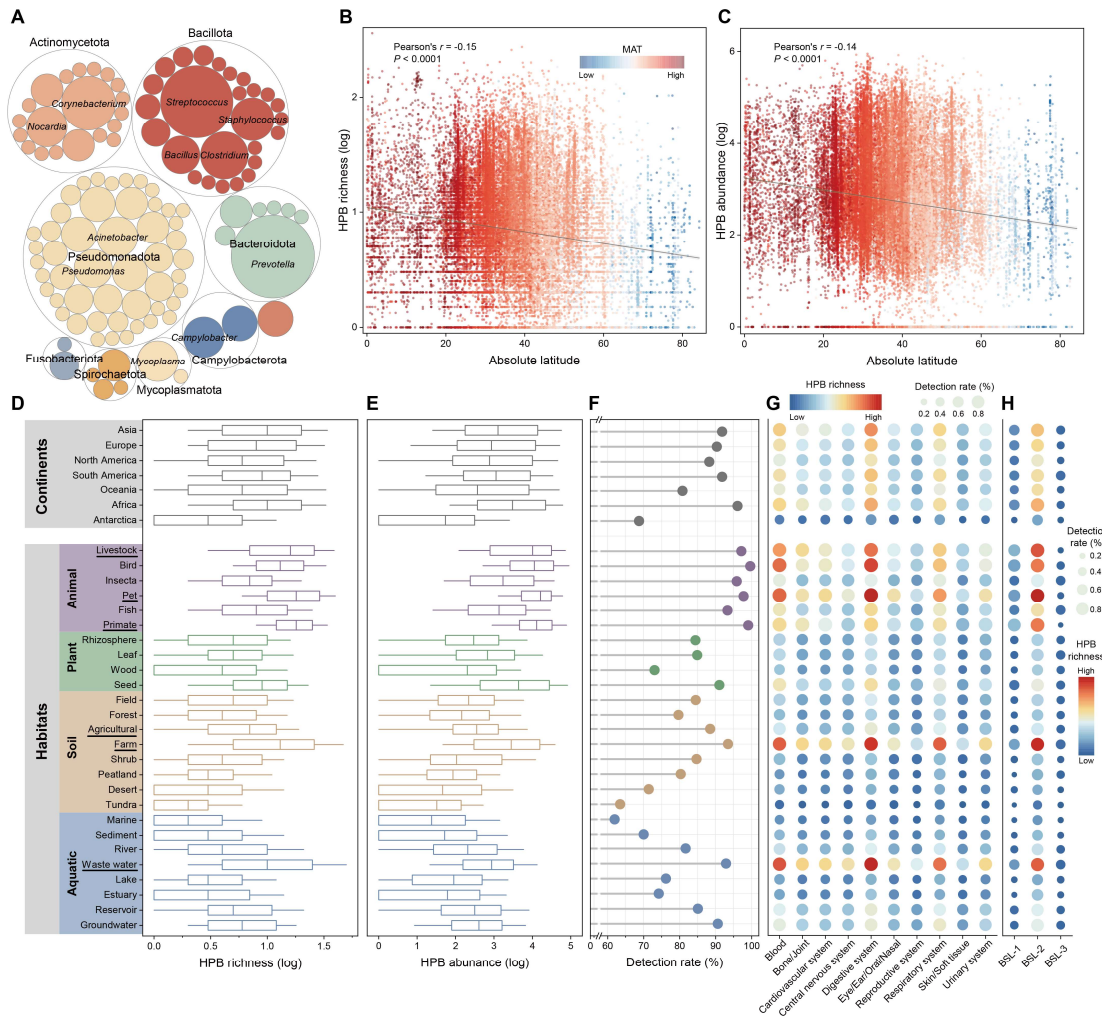
711 Figs. S1 to S17

712 Table S6

713 **Other Supplementary Materials for this manuscript include the following:**

714 Tables S1 to S5

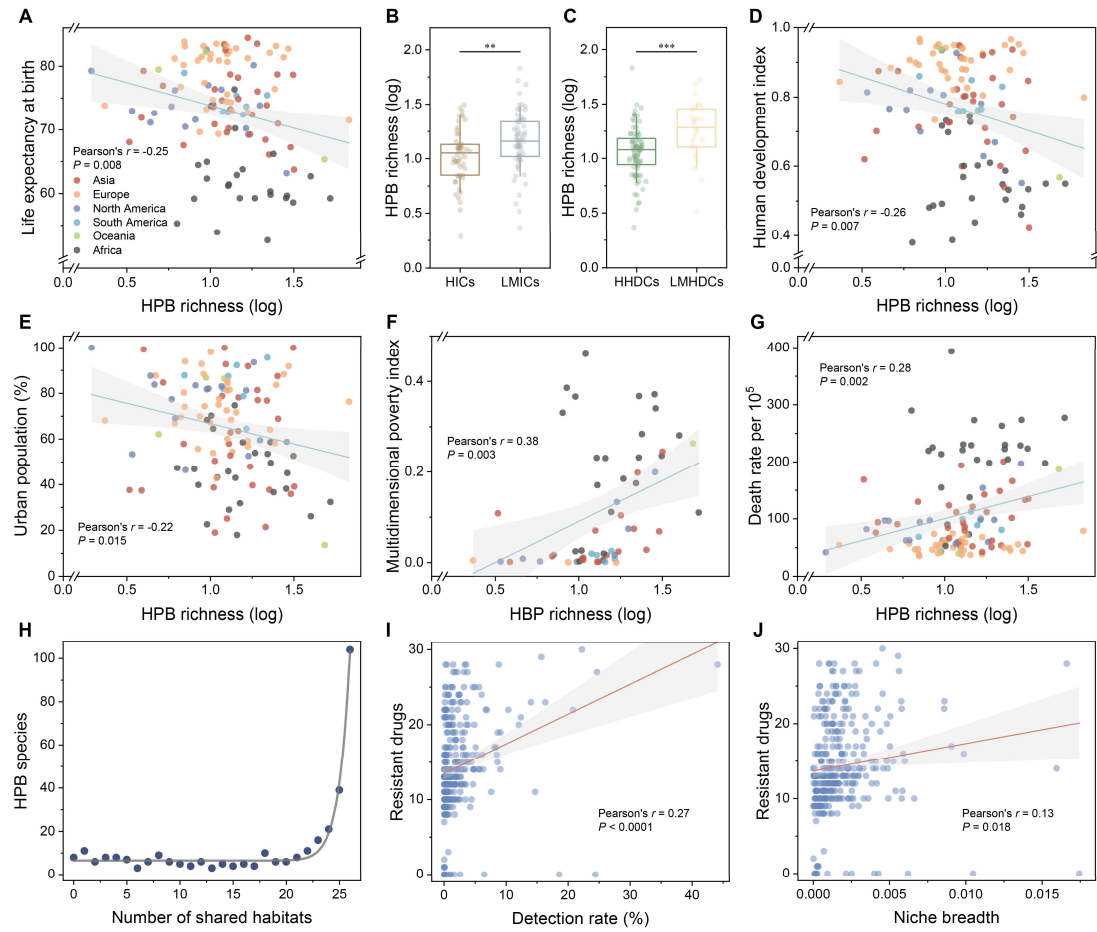
715 **Figures**



716

717 **Fig. 1. Composition and distribution of human pathogenic bacteria (HPB).** (A)  
718 Taxonomy of HPB. The outer and inner circles represent the phyla and genera of HPB,  
719 respectively. The circle size is proportional to the number of species. (B and C)  
720 Latitudinal distributions of the richness (B) and relative abundance (C) of HPB. In all  
721 the depicted scatter plots, the lines indicate the best linear fit, and the shaded areas  
722 represent the 95% confidence intervals of the fitted curves. Pearson's correlation tests  
723 were used to examine the correlation between the richness and abundance of HPB and  
724 absolute latitude, with  $P$  values indicating statistical significance. The color represents  
725 the mean annual temperature (MAT) at the sampling location. (D and E) Richness (D)  
726 and abundance (E) of HPB across continents and habitats. Continents are depicted in  
727 gray, animal-associated habitats in purple, plant-associated habitats in green, soil  
728 habitats in brown, and aquatic habitats in blue. Anthropogenic habitats are underlined.  
729 Each continent contains more than 2,500 samples, and each habitat surpasses 3,500  
730 samples. In all the depicted boxplots, the middle line indicates the median, the box  
731 represents the 25<sup>th</sup>-75<sup>th</sup> percentiles, and the error bar indicates the 10<sup>th</sup>-90<sup>th</sup> percentiles  
732 of the observations. The richness and abundance values are log-transformed (base 10).  
733 (F) Detection rates of HPB across continents and habitats. The detection rate represents

734 the proportion of samples in which HPB was detected to the total number of samples in  
735 each continent or habitat. (**G** and **H**) Pathogenicity (**G**) and biosafety levels (**H**) of HPB  
736 across continents and habitats. There are ten related diseases and three biosafety levels  
737 for HPB. The circle size represents the detection rate of HPB for each pathogenicity or  
738 biosafety level in each continent or habitat, and the color indicates the richness of HPB.

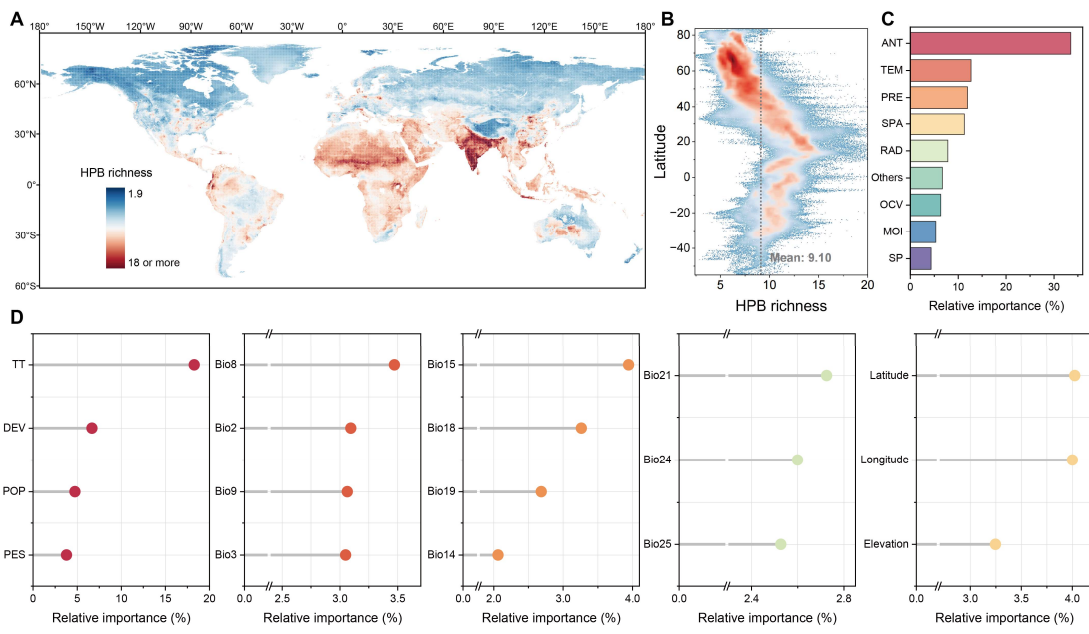


739

740 **Fig. 2. Relationships between the richness of HPB and anthropogenic activities.** (A)  
741 Relationships between the richness of HPB and life expectancy at birth. Each dot  
742 represents a country, and the color indicates the continent where the country is located.  
743 Each country contains more than 30 samples. In all the depicted scatter plots, the lines  
744 indicate the best linear fit, and the shaded areas represent the 95% confidence intervals  
745 of the fitted curves. Pearson's correlation tests were used to examine the correlations,  
746 with  $P$  values indicating statistical significance. Richness values are log-transformed  
747 (base 10). (B) Differences in the richness of HPB among countries with different  
748 income levels. HICs include "High income"; LMICs include "Upper middle income",  
749 "Lower middle income", and "Low income". (C) Differences in the richness of HPB  
750 among countries with different levels of human development. High human  
751 development countries (HHDCs) include "Very high human development" and "High  
752 human development"; low and middle human development countries (LMHDCs)  
753 include "Medium human development", and "Low human development". Comparisons  
754 between bins were conducted using the Wilcoxon rank-sum test,  $**P < 0.01$ ,  $***P <$   
755 0.001. In all the depicted boxplots, the middle line indicates the median, the box  
756 represents the 25<sup>th</sup>-75<sup>th</sup> percentiles, and the error bar indicates the 10<sup>th</sup>-90<sup>th</sup> percentiles  
757 of the observations. (D to G) Relationships between the richness of HPB and  
758 socioeconomic factors. The socioeconomic factors include Human Development Index  
759 (HDI, D), urban population (E), Global Multidimensional Population Index (MPI, F),  
760 and mortality rate per 100,000 by pathogen (G). (H) Cross-habitat distribution of HPB.

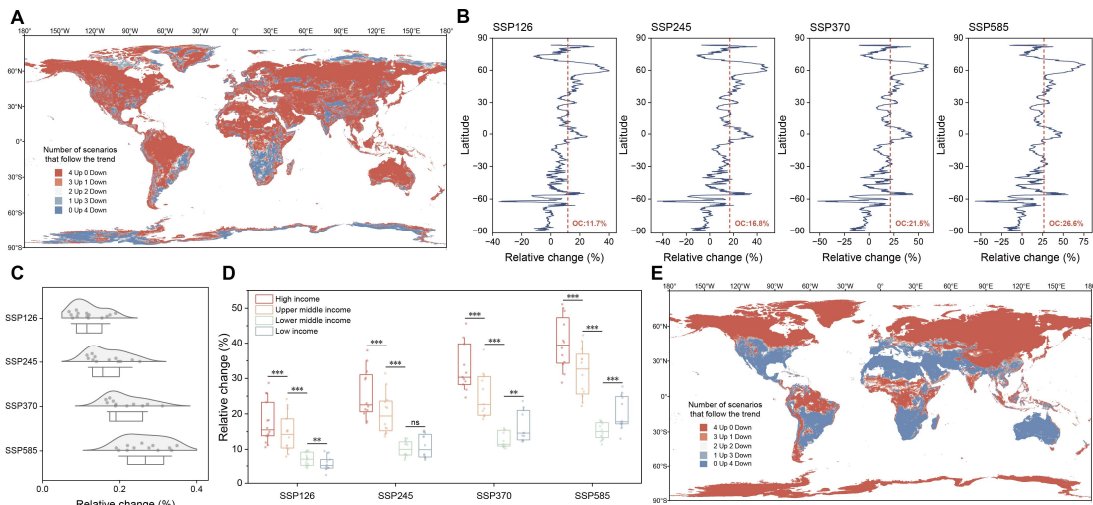
761 The species was considered to be distributed in the habitat only if it appeared in at least  
762 0.1% of the samples. (**I** and **J**) Relationships between the number of resistant drugs and  
763 the average detection rate across different habitats (**I**) or average niche breadth (**J**).

764



765 **Fig. 3. Global pattern of HPB richness.** (A) Global map of the richness of HPB. Using  
 766 covariates, we predicted the richness of HPB globally based on the random forest model.  
 767 (B) Latitudinal distribution of the global richness of HPB. The dashed line represents  
 768 the average richness of HPB worldwide. (C) Relative importance of each major  
 769 category variable in predicting the richness of HPB. ANT: Anthropogenic, TEM:  
 770 Temperature, PRE: Precipitation, SPA: Spatial, RAD: Radiation, OCV: Other climatic  
 771 variables, MOI: Moisture, SP: Soil properties. (D) Relative importance of specific  
 772 variables of anthropogenic, climate, and spatial factors. From left to right, they  
 773 represent ANT, TEM, PRE, RAD, and SPA, respectively. TT: Travel time, DEV:  
 774 Development, POP: Population, PES: Pesticide.

775



776 **Fig. 4. Richness and invasion risk of potential HPB under future climate change**  
777 **scenarios.** (A) Relative changes in HPB richness under future climate change scenarios.  
778 Based on the historical data of 19 bioclimatic variables, a model was constructed using  
779 the random forest algorithm to predict the richness of HPB under current climate  
780 conditions. Using the constructed model, based on future (2080-2100) data of 19  
781 bioclimatic variables, we predicted future HPB richness under four future climate  
782 change scenarios. (B) Latitudinal changes in the richness of HPB under future climate  
783 change scenarios. The dashed line represents the overall change (OC) in HPB richness  
784 under future climate scenarios compared to the current. Shared socioeconomic pathway  
785 (SSP) 126, sustainability; SSP245, middle of the road; SSP370, regional rivalry;  
786 SSP585, fossil-fuelled development. (C) Relative changes in the global richness of  
787 HPB under future climate change scenarios. (D) Relative changes in the richness of  
788 HPB in countries with different income levels under future climate change scenarios.  
789 Comparisons between bins were conducted using the Wilcoxon signed-rank test, ns: not  
790 significant, \*\* $P < 0.01$ , \*\*\* $P < 0.001$ . In all the depicted boxplots, the middle line  
791 indicates the median, the box represents the 25<sup>th</sup>-75<sup>th</sup> percentiles, and the error bar  
792 indicates the 10<sup>th</sup>-90<sup>th</sup> percentiles of the observations. Dots represent the changes in  
793 richness predicted by different global climate models (GCMs) compared to the current  
794 richness. (E) Relative changes in the invasion risk of HPB under future climate change  
795 scenarios. "Up" represents the number of scenarios in which HPB richness or invasion  
796 risk increases, whereas "Down" represents the number of scenarios in which HPB  
797 richness or invasion risk decreases under future climate change scenarios.

Supplementary Materials for  
**Anthropogenic activity and climate change exacerbate the spread of  
pathogenic bacteria in the environment**

Yu Geng *et al.*

\* Corresponding author. Email: liuya@sdu.edu.cn (Y.L.), zhangzheng@sdu.edu.cn (Z.Z.); ORCID:  
0000-0002-1756-0907 (Y.L.), 0000-0001-9971-6006 (Z.Z.)

**This PDF file includes:**

Figs. S1 to S17  
Table S6  
Legends for Tables S1 to S5

**Other Supplementary Materials for this manuscript include the following:**

Tables S1 to S5

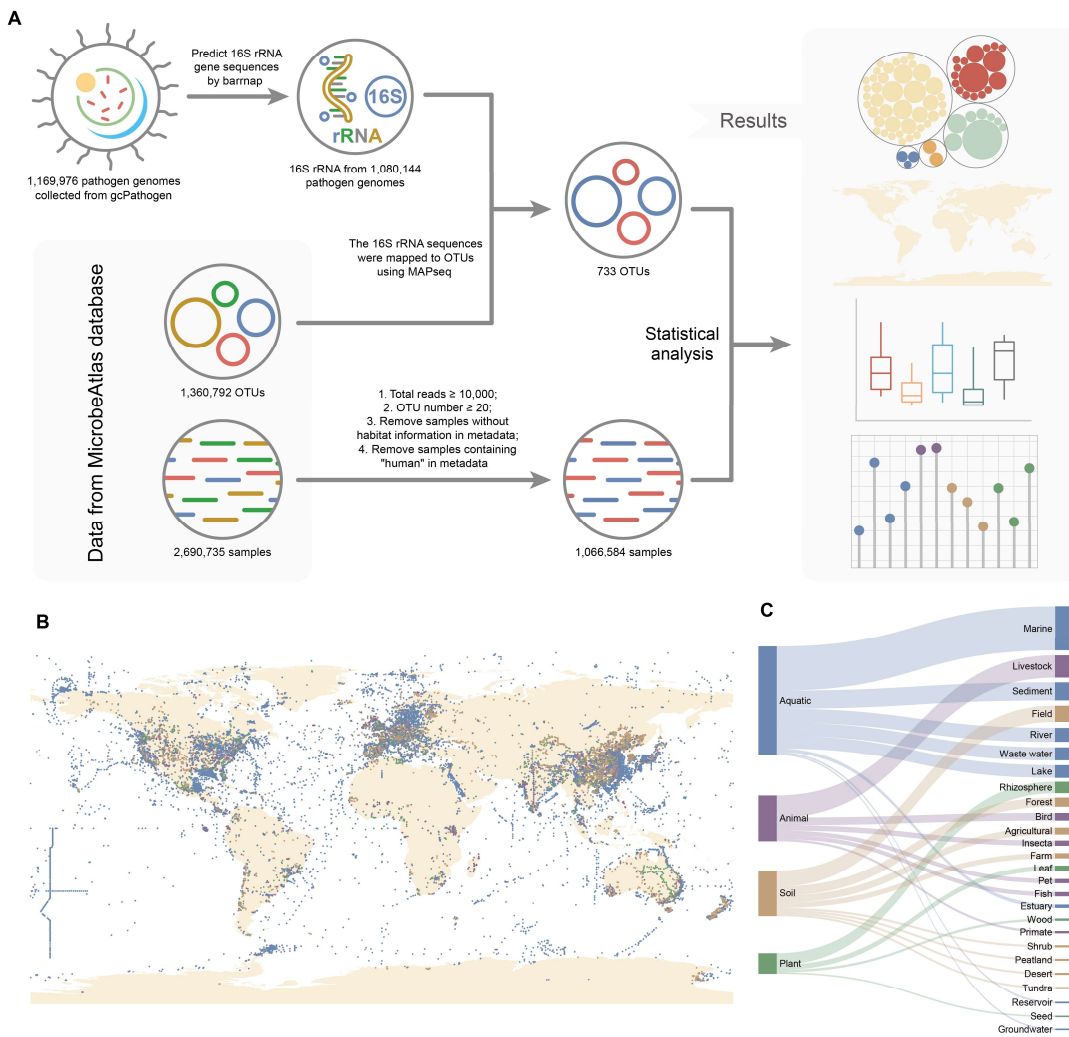


**Fig. S1. Workflow of this study.** (A) Identification process of HPB. (B) Geographical location of the samples. (C) Classification of habitats. Based on the metadata, the samples were classified into four categories: aquatic (blue), animal (purple), soil (brown), and plant (green). Additionally, these categories were further subdivided into 26 distinct microbial habitats.

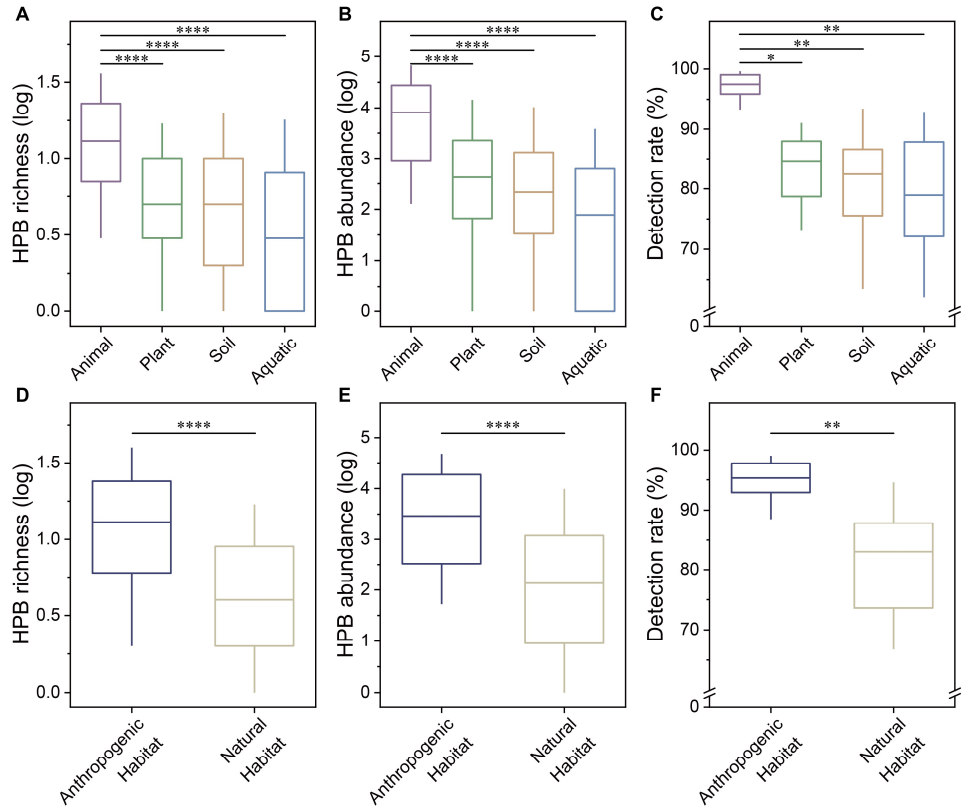


**Fig. S2. HPB in different types of habitats.** (A to C) Differences in HPB richness (A), abundance (B), and detection rates (C) across four habitats: animal, plant, soil, and aquatic. (D to F) Differences in HPB richness (D), abundance (E), and detection rates (F) between anthropogenic habitats and natural habitats. Comparisons between bins were conducted using the Wilcoxon rank-sum test,  $*P < 0.05$ ,  $**P < 0.01$ ,  $****P < 0.0001$ . In all the depicted boxplots, the middle line indicates the median, the box represents the 25<sup>th</sup>-75<sup>th</sup> percentiles, and the error bar indicates the 10<sup>th</sup>-90<sup>th</sup> percentiles of the observations. The richness and abundance values are log-transformed (base 10).

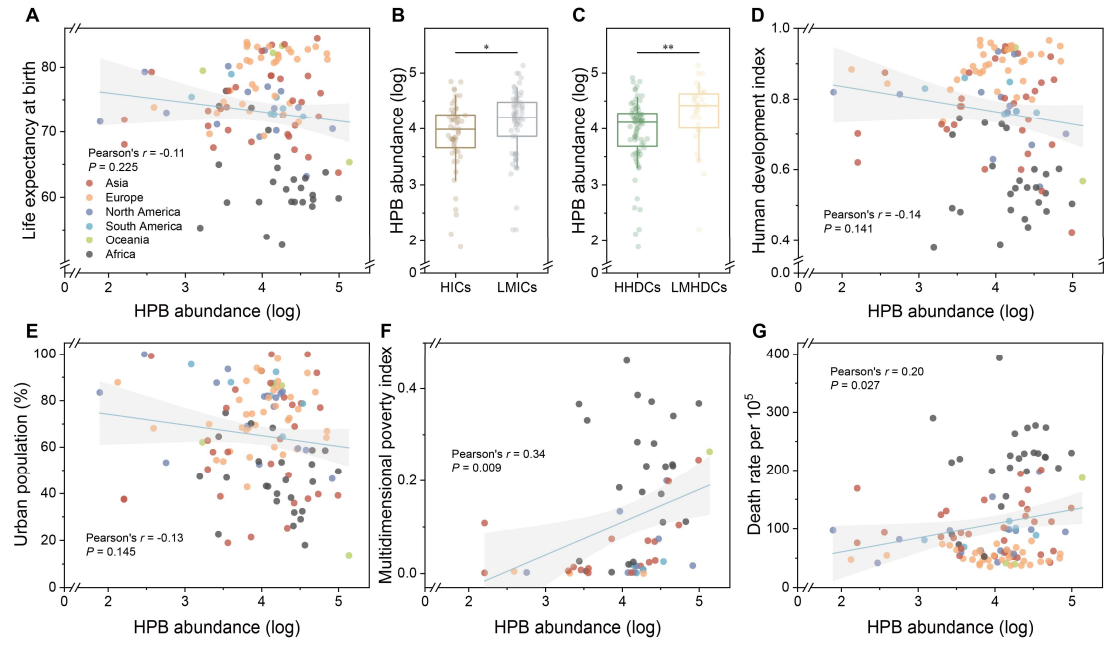


**Fig. S3. Relationships between the abundance of HPB and anthropogenic activities.** (A) Relationships between the abundance of HPB and life expectancy at birth (2022). Each dot represents a country, and the color indicates the continent where the country is located. Each country contains more than 30 samples. In all the depicted scatter plots, the lines indicate the best linear fit, and the shaded areas represent the 95% confidence intervals of the fitted curves. Pearson's correlation tests were used to examine the correlations, with  $P$  values indicating statistical significance. Abundance values are log-transformed (base 10). (B) Differences in the abundance of HPB among countries with different income levels (2024 fiscal year). High-income countries (HICs) are shown in brown, including "High income"; low- and middle-income countries (LMICs) are shown in gray, including "Upper middle income", "Lower middle income", and "Low income". (C) Differences in the abundance of HPB among countries with different levels of human development (2024). High human development countries (HHDCs) are shown in green, including "Very high human development" and "High human development"; low and middle human development countries (LMHDCs) are shown in light yellow, including "Medium human development" and "Low human development". Comparisons between bins were conducted using the Wilcoxon rank-sum test, \* $P < 0.05$ , \*\* $P < 0.01$ . In all the depicted boxplots, the middle line indicates the median, the box represents the 25<sup>th</sup>-75<sup>th</sup> percentiles, and the error bar indicates the 10<sup>th</sup>-90<sup>th</sup> percentiles of the observations. (D to G) Relationships between the abundance of HPB and socioeconomic factors. The socioeconomic factors include Human Development Index (HDI, 2024, D), urban population (2022, E), Global Multidimensional Population Index (MPI, 2023, F), and mortality rate per 100,000 by pathogen (2019, G).

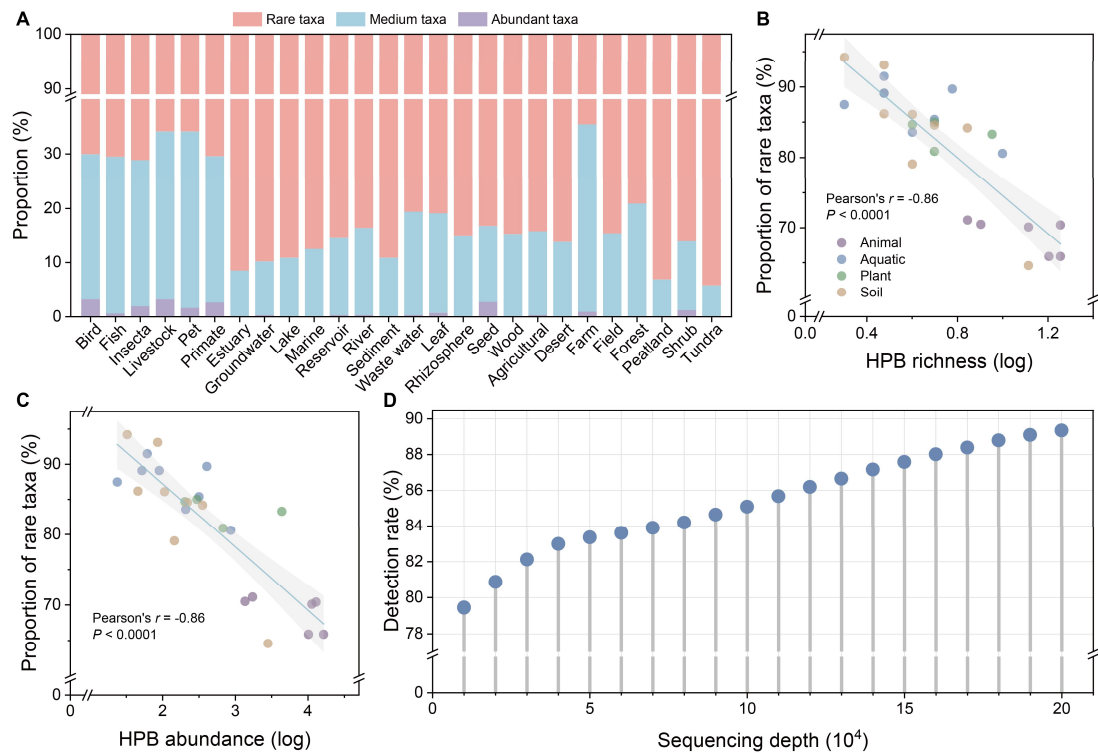


**Fig. S4. HPB in the natural environment are mainly composed of rare taxa.** (A) Proportions of various taxa of HPB in different habitats. Rare taxa (species with a relative sequence abundance  $< 0.001\%$  across all samples of a habitat) are shown in red, medium taxa (species with a relative sequence abundance between  $0.001\%$  and  $0.1\%$  across all samples of a habitat) are shown in blue, and abundant taxa (species with a relative sequence abundance  $\geq 0.1\%$  across all samples of a habitat) are shown in purple. (B and C) Relationships between the richness (B) and abundance (C) of HPB and the proportions of rare taxa. Each dot represents a habitat type. In all the depicted scatter plots, the lines indicate the best linear fit, and the shaded areas represent the 95% confidence intervals of the fitted curves. Pearson's correlation tests were used to examine the correlation between the richness and abundance of HPB and the proportion of rare taxa, with  $P$  values indicating statistical significance. The richness and abundance values are log-transformed (base 10). (D) Relationship between sequencing depth and the HPB detection rate.

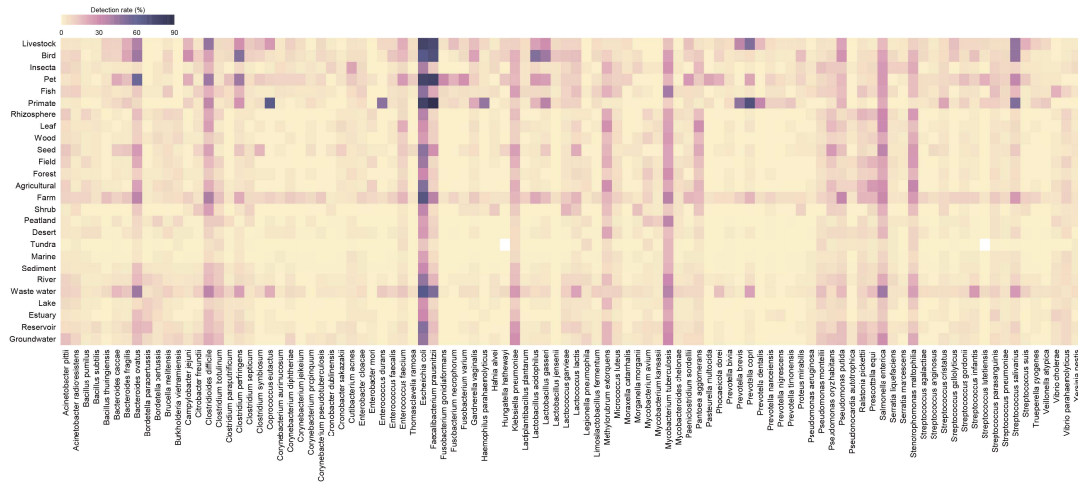


**Fig. S5. Detection rates of HPB species in each habitat.** The HPB species were selected based on the top 100 average detection rates of 26 habitats.

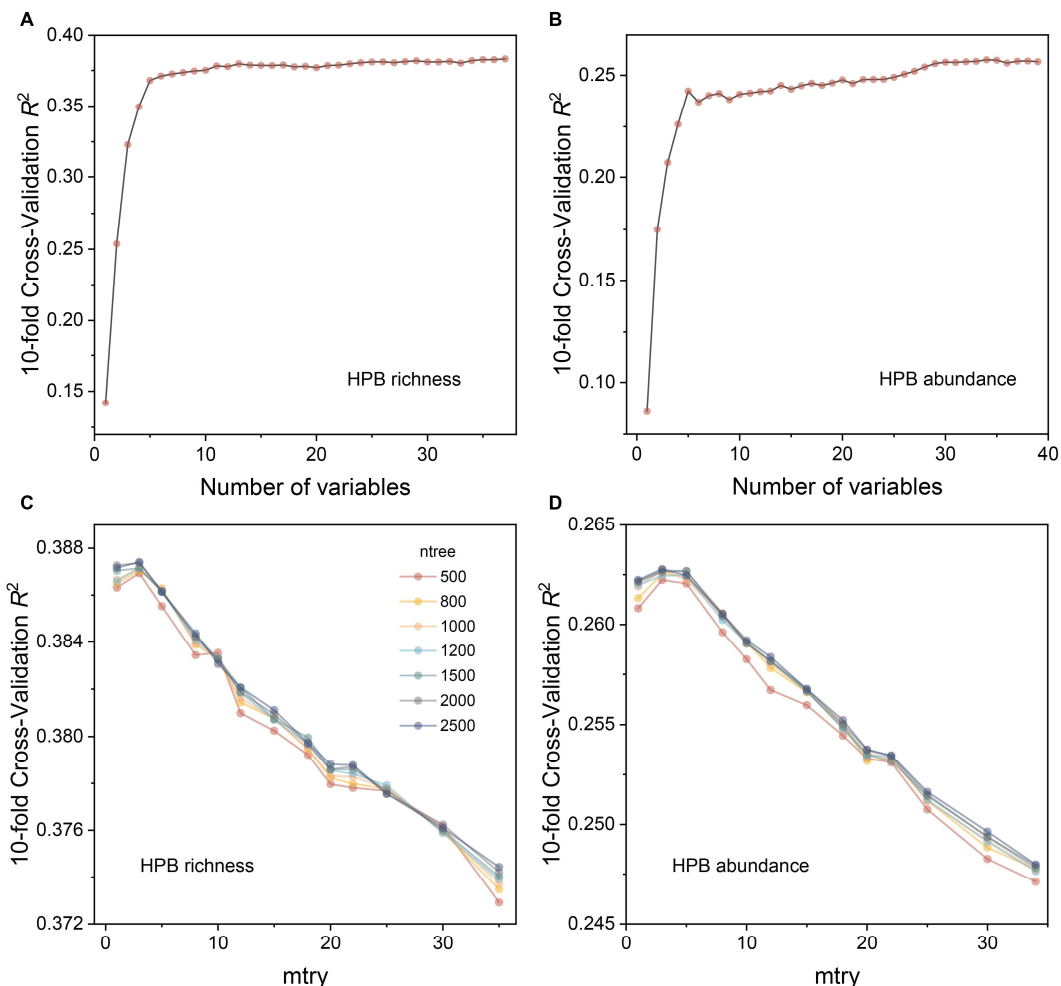


**Fig. S6. Feature selection and hyperparameter tuning for machine learning.** (A and B) Feature selection for the random forest algorithm was performed using recursive feature elimination and 10-fold cross-validation to identify the optimal set of variables for predicting the richness (A) and abundance (B) of HPB. (C and D) Hyperparameter tuning for the random forest algorithm was conducted using grid search and 10-fold cross-validation to select the optimal combination of hyperparameters for predicting the richness (C) and abundance (D) of HPB.

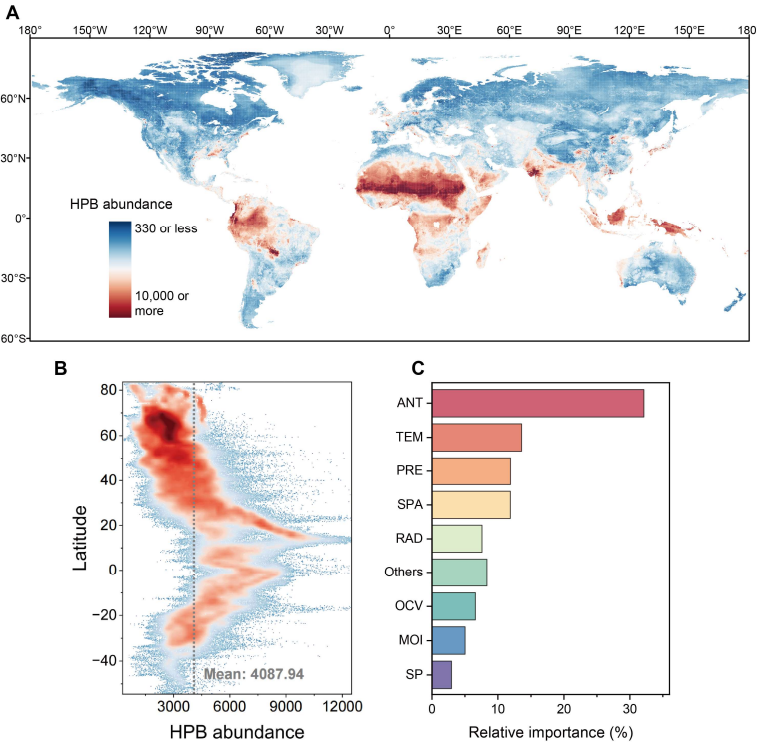


**Fig. S7. Global pattern of HPB abundance.** (A) Global map of the abundance of HPB. Using covariates, we predicted the abundance of HPB globally based on the random forest model. (B) Latitudinal distribution of the global abundance of HPB. The dashed line represents the average abundance of HPB worldwide. (C) Relative importance of each major category variable in predicting the abundance of HPB. ANT: Anthropogenic, TEM: Temperature, PRE: Precipitation, SPA: Spatial, RAD: Radiation, OCV: Other climatic variables, MOI: Moisture, SP: Soil properties.

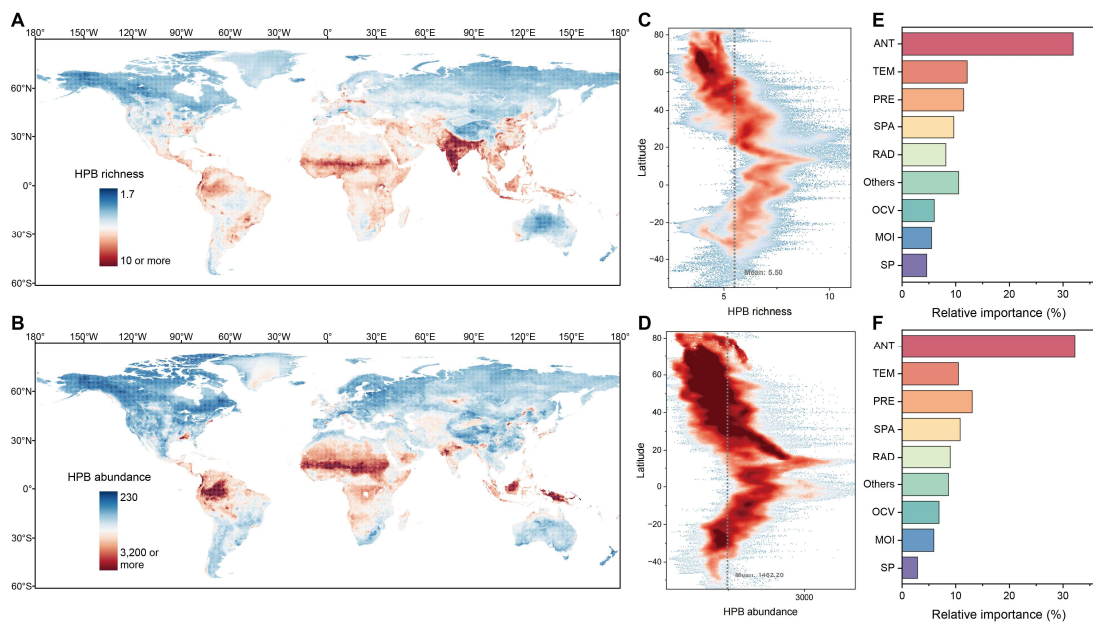


**Fig. S8. Global patterns of the richness and abundance of HPB excluding common commensal and opportunistic pathogenic bacteria.** (A and B) Global map of the richness (A) and abundance (B) of HPB excluding common commensal and opportunistic pathogenic bacteria. (C and D) Latitudinal distributions of the global richness (C) and abundance (D) of HPB excluding common commensal and opportunistic pathogenic bacteria. The dashed line represents the average richness or abundance of HPB worldwide. (E and F) Relative importance of each major category variable in predicting the richness (E) and abundance (F) of HPB excluding common commensal and opportunistic pathogenic bacteria. ANT: Anthropogenic, TEM: Temperature, PRE: Precipitation, SPA: Spatial, RAD: Radiation, OCV: Other climatic variables, MOI: Moisture, SP: Soil properties. The removed common commensal and opportunistic pathogenic bacteria include: *Escherichia coli*, *Salmonella enterica*, *Faecalibacterium prausnitzii*, *Clostridioides difficile*, *Staphylococcus aureus*, *Enterococcus faecium*, *Prevotella copri*, *Corynebacterium jeikeium*, *Serratia marcescens*, *Legionella pneumophila*, *Mycobacterium avium*, *M. tuberculosis*, *Pseudomonas aeruginosa*, *P. putida*, *Streptococcus pyogenes*, *S. pneumoniae*, and *S. parasanguinis*.

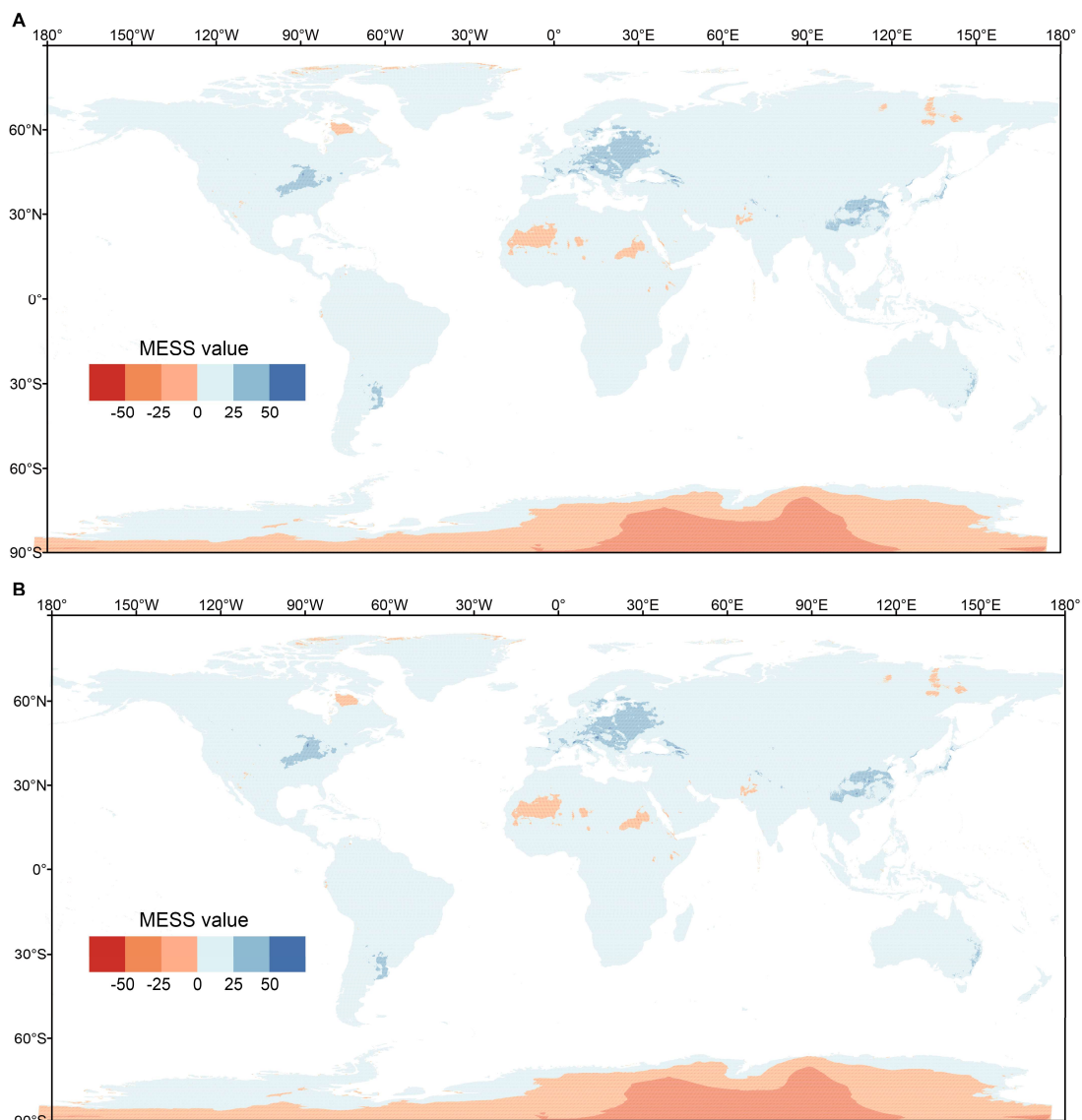


**Fig. S9. Multivariate environmental similarity surface (MESS) analysis.** (A and B) Extrapolation reliability of the samples was evaluated through MESS analysis. The higher MESS value indicates high extrapolation reliability.

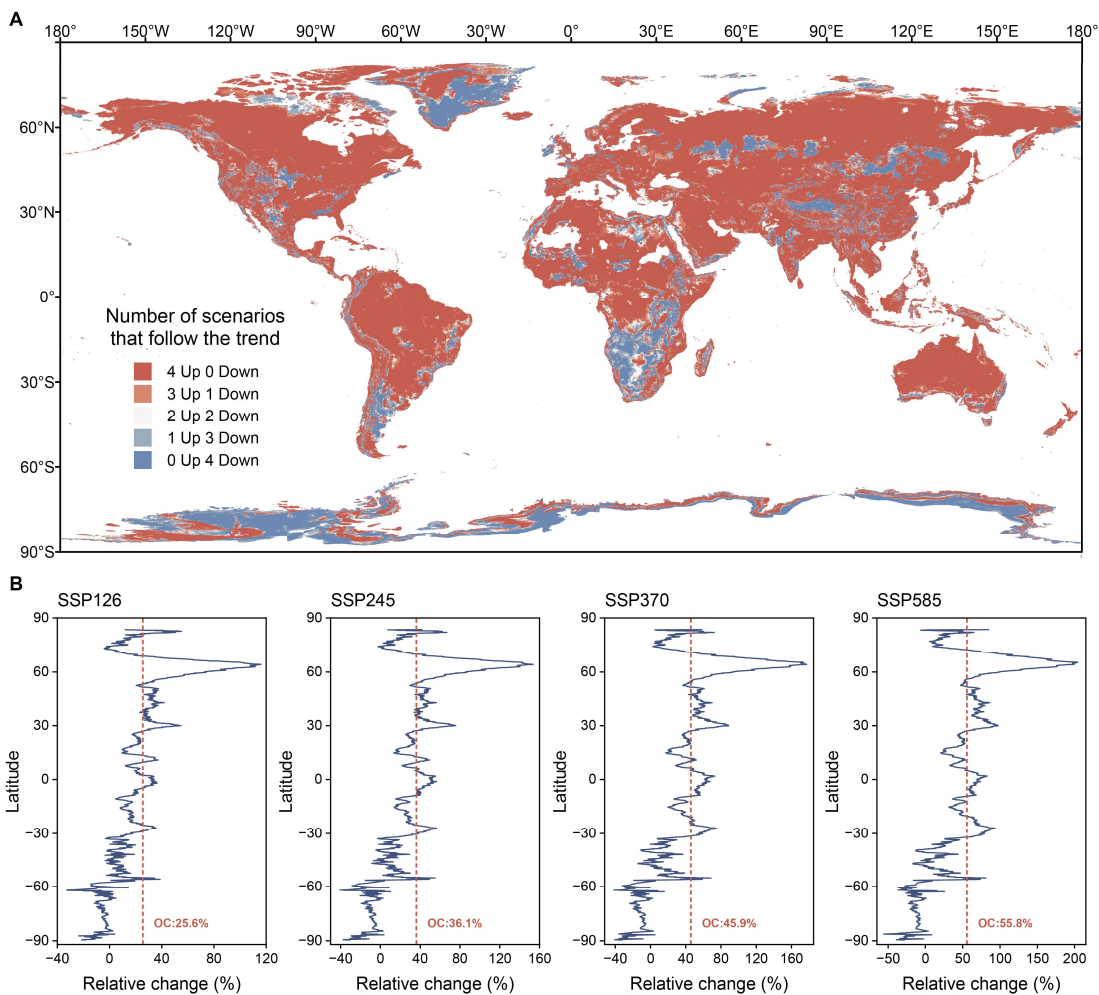


**Fig. S10. Abundance of potential HPB under future climate change scenarios.** (A) Relative changes in HPB abundance under future climate change scenarios. Based on the historical data of 19 bioclimatic variables, a model was constructed using the random forest algorithm to predict the abundance of HPB under current climate conditions. Using the constructed model, based on future (2080-2100) data of 19 bioclimatic variables, we predicted future HPB abundance under four future climate change scenarios. "Up" represents the number of scenarios in which the HPB abundance increases, whereas "Down" represents the number of scenarios in which the HPB abundance decreases under future climate change scenarios. (B) Latitudinal changes in the abundance of HPB under future climate change scenarios. The dashed line represents the overall change (OC) in HPB abundance under future climate scenarios compared to the current. Shared socioeconomic pathway (SSP) 126, sustainability; SSP245, middle of the road; SSP370, regional rivalry; SSP585, fossil-fuelled development.

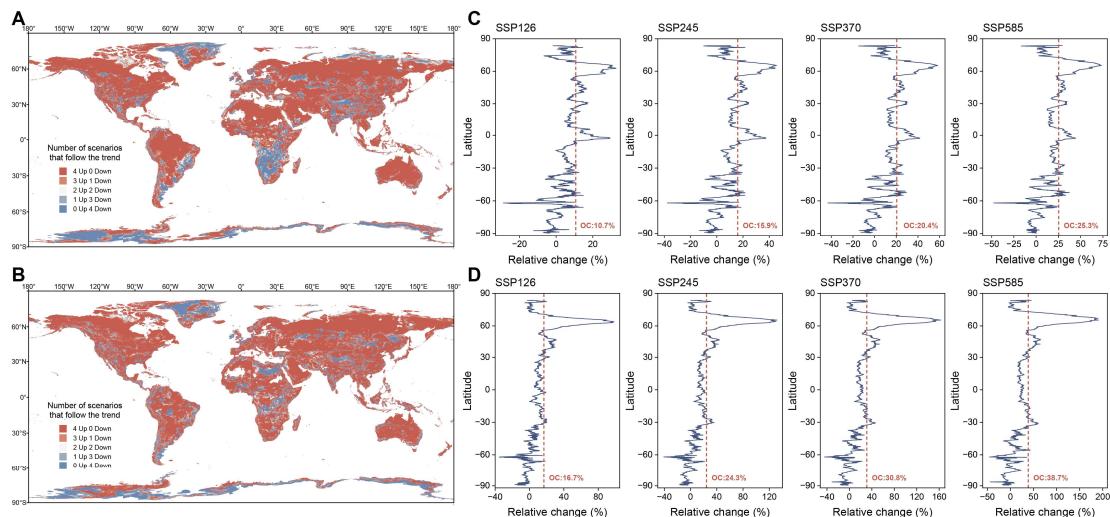


**Fig. S11. Richness and abundance of potential HPB excluding common commensal and opportunistic pathogenic bacteria under future climate change scenarios.** (A and B) Relative changes in the richness (A) and abundance (B) of HPB excluding common commensal and opportunistic pathogenic bacteria under future climate change scenarios. Based on the historical data of 19 bioclimatic variables, models were constructed using the random forest algorithm to predict the richness and abundance of HPB excluding common commensal and opportunistic pathogenic bacteria under current climate conditions. Using the constructed models, based on future (2080-2100) data of 19 bioclimatic variables, we predicted future the richness and abundance of HPB excluding common commensal and opportunistic pathogenic bacteria under four future climate change scenarios. "Up" represents the number of scenarios in which HPB richness or abundance increases, whereas "Down" represents the number of scenarios in which HPB richness or abundance decreases under future climate change scenarios. (C and D) Latitudinal changes in the richness (C) and abundance (D) of HPB excluding common commensal and opportunistic pathogenic bacteria under future climate change scenarios. The dashed line represents the overall change (OC) in HPB richness or abundance under future climate scenarios compared to the current. Shared socioeconomic pathway (SSP) 126, sustainability; SSP245, middle of the road; SSP370, regional rivalry; SSP585, fossil-fuelled development.

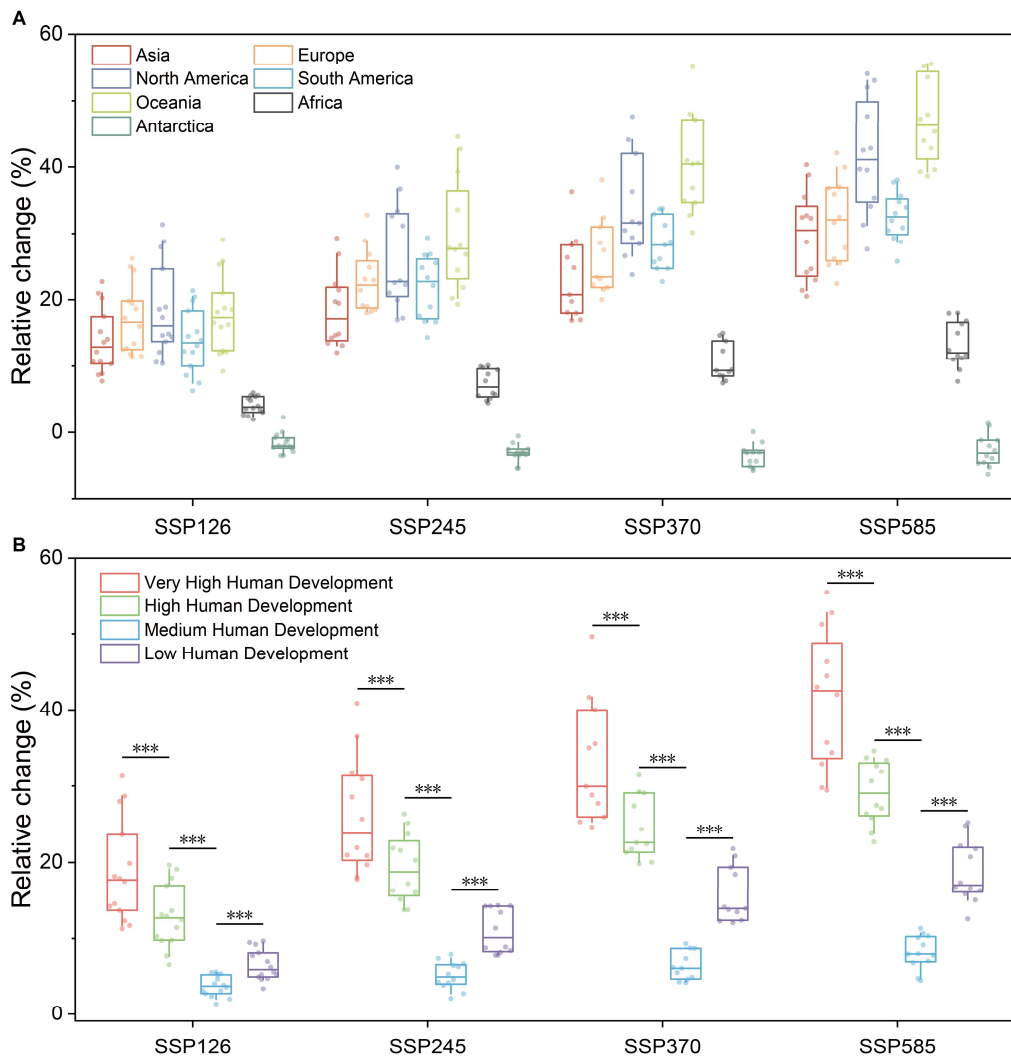


**Fig. S12. Relative changes in HPB richness in different regions under future climate change scenarios.** (A) Relative changes in the richness of HPB on different continents under future climate change scenarios. (B) Relative changes in the richness of HPB in countries with different human development levels under future climate change scenarios. Comparisons between bins were conducted using the Wilcoxon signed-rank test, \*\*\* $P < 0.001$ . In all the depicted boxplots, the middle line indicates the median, the box represents the 25<sup>th</sup>-75<sup>th</sup> percentiles, and the error bar indicates the 10<sup>th</sup>-90<sup>th</sup> percentiles of the observations. Dots represent the changes in richness predicted by different GCMs compared to the current richness.

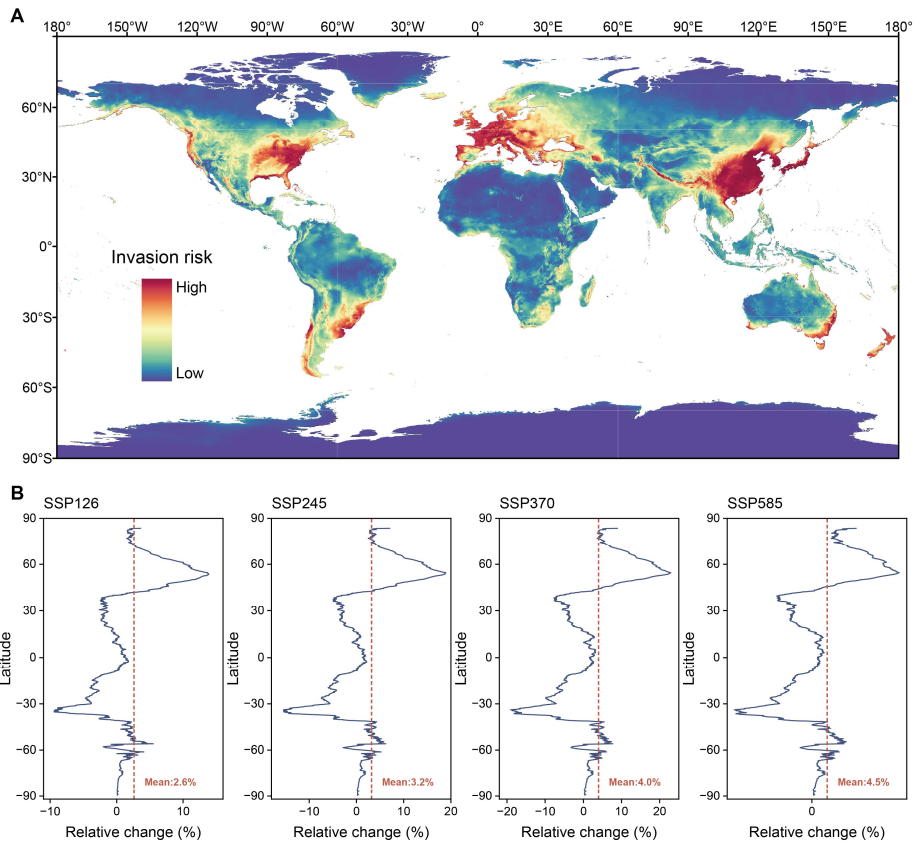


**Fig. S13. Global invasion risk of potential HPB.** (A) Predicted global invasion risk of potential HPB under current climate conditions. (B) Latitudinal changes in the invasion risk of HPB under future climate change scenarios. The dashed line represents the average change in the invasion risk of HPB under future climate scenarios compared to the current.

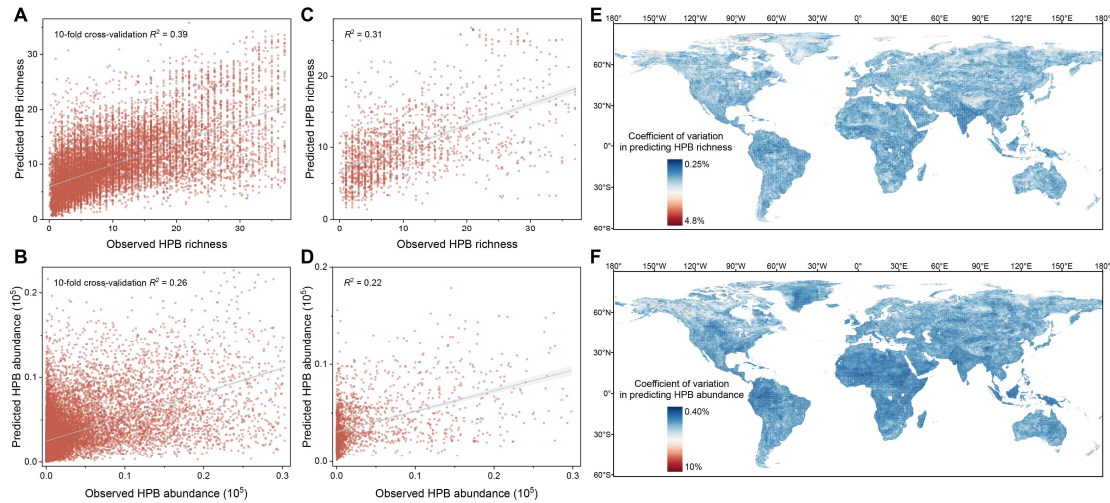


**Fig. S14. Evaluation of machine learning models for global distribution.** **(A)** Relationship between the predicted and observed richness in the training set. **(B)** Relationship between the predicted and observed abundance in the training set. The performance of the model on the training set was evaluated through 10-fold cross-validation  $R^2$ . **(C)** Relationship between the predicted and observed richness in the testing set. **(D)** Relationship between the predicted and observed abundance in the testing set. The performance of the model on the testing set was evaluated through  $R^2$ . **(E and F)** Coefficients of variation were used to evaluate the uncertainty of the predicted global HPB richness (E) and abundance (F).

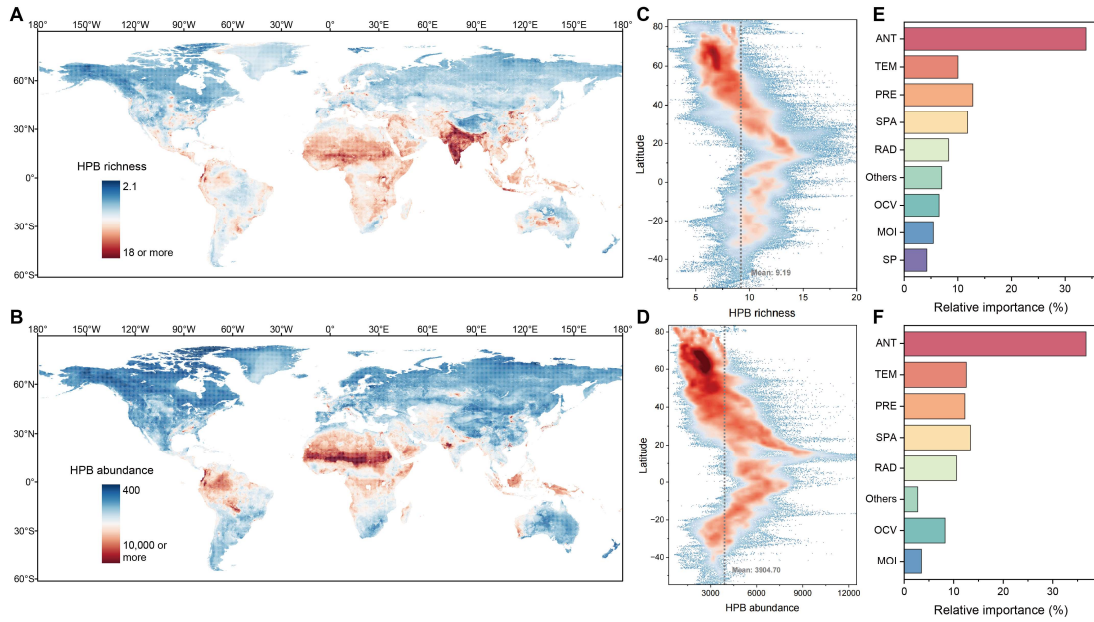


**Fig. S15. Global patterns of HPB richness and abundance predicted through spatial cross-validation.** (A and B) Global map of the richness (A) and abundance (B) of HPB. Using the random forest algorithm, we predicted the richness and abundance of HPB globally based on spatial cross-validation. (C and D) Latitudinal distributions of the global richness (C) and abundance (D) of HPB. The dashed line represents the average richness or abundance of HPB worldwide. (E and F) Relative importance of each major category variable in predicting the richness (E) and abundance (F) of HPB. ANT: Anthropogenic, TEM: Temperature, PRE: Precipitation, SPA: Spatial, RAD: Radiation, OCV: Other climatic variables, MOI: Moisture, SP: Soil properties.

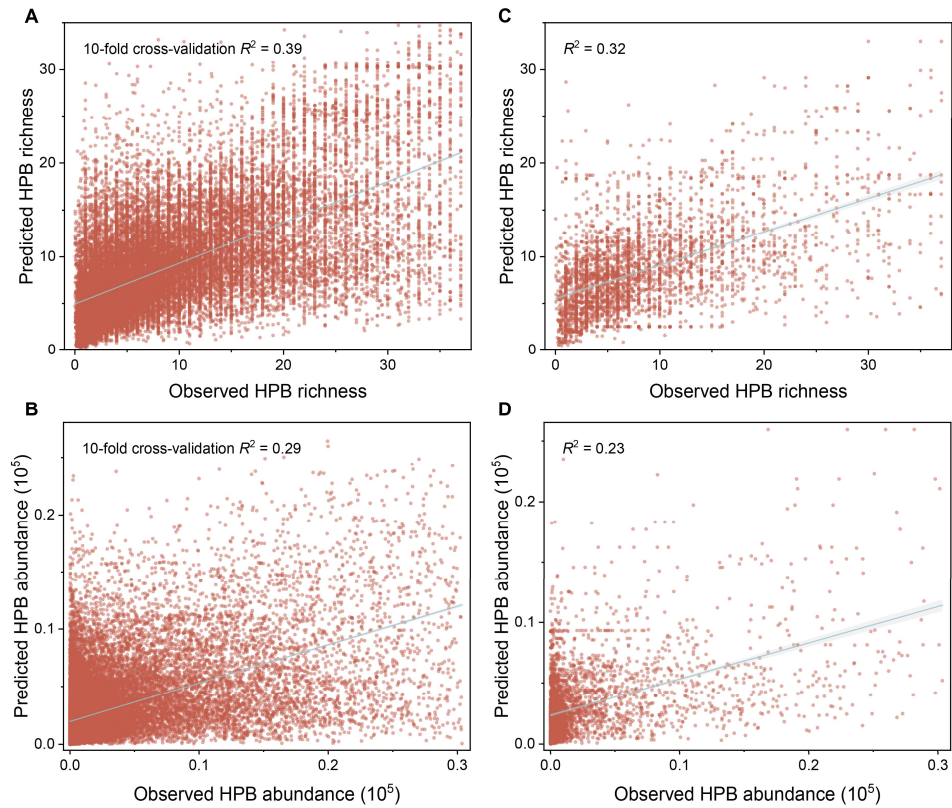


**Fig. S16. Evaluation of machine learning models for climate change.** **(A)** Relationship between the predicted and observed richness in the training set for climate change. **(B)** Relationship between the predicted and observed abundance in the training set for climate change. The performance of the model on the training set was evaluated through 10-fold cross-validation  $R^2$ . **(C)** Relationship between the predicted and observed richness in the testing set for climate change. **(D)** Relationship between the predicted and observed abundance in the testing set for climate change. The performance of the model on the testing set was evaluated through  $R^2$ .

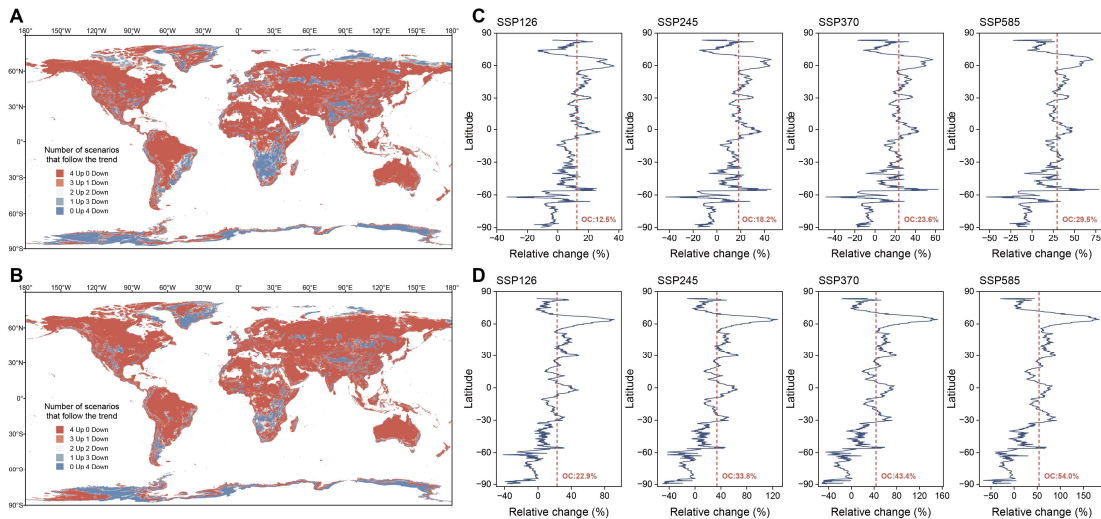


**Fig. S17. Richness and abundance of potential HPB predicted through spatial cross-validation under future climate change scenarios.** (A and B) Relative changes in HPB richness (A) and abundance (B) under future climate change scenarios. Based on the historical data of 19 bioclimatic variables, models were constructed using the random forest algorithm to predict the richness and abundance of HPB under current climate conditions. The construction of the models is based on spatial cross-validation. Using the constructed model, based on future (2080-2100) data of 19 bioclimatic variables, we predicted future HPB richness and abundance under four future climate change scenarios. "Up" represents the number of scenarios in which HPB richness or abundance increases, whereas "Down" represents the number of scenarios in which HPB richness or abundance decreases under future climate change scenarios. (C and D) Latitudinal changes in the richness (C) and abundance (D) of HPB under future climate change scenarios. The dashed line represents the overall change (OC) in HPB richness or abundance under future climate scenarios compared to the current. Shared socioeconomic pathway (SSP) 126, sustainability; SSP245, middle of the road; SSP370, regional rivalry; SSP585, fossil-fuelled development.

**Table S6** Future climate models used in the current study

<b>Model name</b>	<b>SSP126</b>	<b>SSP245</b>	<b>SSP370</b>	<b>SSP585</b>
ACCESS-CM2	√	√	√	√
BCC-CSM2-MR	√	✗	✗	✗
CMCC-ESM2	√	√	√	√
EC-Earth3-Veg	√	√	√	√
FIO-ESM-2-0	√	√	✗	√
GFDL-ESM4	√	✗	√	✗
GISS-E2-1-G	√	√	√	√
HadGEM3-GC31-LL	√	√	✗	√
INM-CM5-0	√	√	√	√
IPSL-CM6A-LR	√	√	√	√
MIROC6	√	√	√	√
MPI-ESM1-2-HR	√	√	√	√
MRI-ESM2-0	√	√	√	√
UKESM1-0-LL	√	√	√	√

**Other Supplementary Materials for this manuscript include the following:**

**Table S1** Taxonomic information of human pathogenic bacteria

**Table S2** Socioeconomic factors of each country

**Table S3** The covariates used in machine learning

**Table S4** The relative importance of variables in predicting the richness of human pathogenic bacteria

**Table S5** The relative importance of variables in predicting the abundance of human pathogenic bacteria